# Statistical Mechanics of Coil-rod Structure in Biopolymer Gels

Hashem Moosavian[a], Tian Tang[a,*]

[a]*Department of Mechanical Engineering, University of Alberta, Edmonton, T6G 1H9, Alberta, Canada*

**Abstract**

Due to the unique properties of biopolymer gels, they are extensively used in the food industry and biomedical applications such as drug delivery. Different from rubber-like materials, the constituting chains in many biopolymer gels randomly interlock with neighbouring chains by means of physical rather than covalent cross-linking. Such polymer networks are characterized by two principal regions: the disordered zone containing coiled chains and the ordered zone in the form of ion-mediated aggregation of macromolecules and/or helical structures. The ordered regions serve as junction zones between the disordered chains, and the size of these zones may alter as a result of zipping/unzipping phenomena. The entire polymer network can be envisaged as a collection of coil-rod structures serving as the building blocks, where the coil and rod are representative of the disordered and ordered zones, respectively. The present work aims to provide a rigorous formulation of coil-rod structure that can predict its mechanical behaviour including zipping/unzipping characteristics. The coil-rod structure is modelled by a rod attached to a freely jointed chain, where the length of the rod and the number of segments in the freely jointed chain are adjustable input parameters. The relationship between the force and end-to-end distance of the coil-rod structure is derived based on statistical mechanics. The formulation is extended to incorporate the zipping/unzipping

*Corresponding author

*Email address:* tian.tang@ualberta.ca (Tian Tang )

mechanism with the aid of Boltzmann averaging. As an example of its applications, the model is implemented into the eight-chain model to describe the macroscopic mechanical response of the network. Another example is demonstrated where the zipping/unzipping mechanism is shown to be able to capture the unwinding of a double-stranded DNA under a tensile force. The formulation presented in this work paves the way for future studies that model biopolymer gel networks with potentially complex chain interactions.
*Keywords:* Biopolymer gels, Zipping mechanism, Coil-rod structure, Statistical mechanics, Partition function, Force-extension relationship

---

## Nomenclature

| | |
|---|---|
| $\Psi$ | Helmholtz free energy per unit reference volume |
| $\lambda_1$, $\lambda_2$, $\lambda_3$ | Principal stretches |
| $\mathscr{N}$ | Number of chains per unit reference volume |
| $\mu$ | Shear modulus |
| $\psi_i$ | Helmholtz free energy of the $i$th chain per unit reference volume |
| $\sigma_1$, $\sigma_2$, $\sigma_3$ | Principal Cauchy stresses |
| $p_0$ | Unknown pressure in (49) |
| $r_0$ | End-to-end distance of the chain in the reference configuration |
| $r_{\text{chain}}$ | End-to-end distance of the chain in the current configuration |
| $A_0$ | Normalization factor in the probability distribution (33) |
| $G$ | Gibbs free energy |
| $M$ | Total number of segments in the structure |
| $N$ | Number of Kuhn segments in the fully unwound coil-rod structure |
| $Q(f_x, T, M)$ | Isothermal-isotension partition function with fixed applied force $f_x$ in $x$ direction, |

| | |
|---|---|
| | temperature, and number of segments |
| $Q^{\mathrm{R}}(f_x, T)$ | Isothermal-isotension partition function of the rod with fixed applied force $f_x$ in $x$ direction and temperature |
| $Q^{\mathrm{W}}(f_x, T)$ | Isothermal-isotension partition function of the Weiner's rigid model for the rod structure with fixed applied force $f_x$ in $x$ direction and temperature |
| $T$ | Temperature |
| $W(\boldsymbol{r})$ | The probability that the end-to-end vector of the structure is $\boldsymbol{r}$, at fixed temperature and number of segments |
| $W_n^{\mathrm{CR}}(\boldsymbol{r})$ | The probability that the end-to-end vector of the coil-rod structure is $\boldsymbol{r}$, with fixed temperature and number of Kuhn segments $n$ in the coil |
| $Z(\boldsymbol{r}, T, M)$ | The canonical partition function with fixed end-to-end position vector, temperature, and number of segments |
| $Z(x, T, M)$ | The canonical partition function with fixed end-to-end distance in $x$ direction, temperature, and number of segments |
| $Z^{\mathrm{R}}(x, T)$ | The canonical partition function of the rod with fixed end-to-end projection in $x$ direction and temperature |
| $Z^{\mathrm{W}}(x, T)$ | The canonical partition function of the Weiner's rigid model for the rod with fixed end-to-end projection in $x$ direction and temperature |
| $Z_0$ | The integration of canonical partition function over the entire space, Eq. (6) |
| $\boldsymbol{r}$ | End-to-end position vector of the coil-rod structure |
| $\langle x \rangle$ | Average end-to-end distance in $x-$direction due to the application of a fixed force $f_x$ on the ends |
| $\langle f_r \rangle$ | Average force required to maintain the structure at fixed end-to-end distance $r$ |
| $\langle f_x \rangle$ | Average force required to maintain the structure at fixed end-to-end distance along |

| | |
|---|---|
| | $x-$direction |
| $\mathrm{d}\tau$ | An arbitrary volume element in the space |
| $\mathscr{H}$ | The governing Hamiltonian of the system |
| $a$ | Unstretched length of the rod |
| $b$ | Kuhn length of the coil |
| $h$ | Planck's constant |
| $k_B$ | The Boltzmann constant |
| $m$ | Mass of the end points in the rod model |
| $n$ | Number of Kuhn segments in the coil |
| $n_0(\boldsymbol{r})$ | Number of Kuhn segments with maximum contribution to the summation (43) |
| $n_{\max}$ | Maximum number of Kuhn segments in the coil during zipping/unzipping |
| $n_{\min}$ | Minimum number of Kuhn segments in the coil during zipping/unzipping |
| $p(x)$ | The probability that the two ends of the structure are separated by $x$ in the $x$ direction at constant temperature |
| $p_n^{\mathrm{CR}}(x)$ | The probability that the two ends of the coil-rod structure are separated by $x$ in the $x$ direction at constant temperature |
| $p_n^{\mathrm{C}}(x)$ | The probability that the two ends of the coil structure are separated by $x$ in the $x$ direction at constant temperature |
| $p_x$, $p_y$, $p_z$ | Components of the momentum vector of the rod end along $x$, $y$ and $z$ direction |
| $q_x$, $q_y$, $q_z$ | Components of the position vector of the rod end along $x$, $y$ and $z$ direction |
| $r$ | End-to-end distance of the structure |
| $r^*$ | The end-to-end distance with maximum probability |
| $\Delta l$ | An arbitrary factor of length dimension for normalization purpose |
| $\Omega(\boldsymbol{r}, T, \varepsilon)$ | The grand canonical partition function with fixed end-to-end position vector, tem- |

| | |
|---|---|
| | perature, and chemical potential |
| $\Phi$ | Grand canonical potential energy |
| $\alpha$ | Ratio of the length of one unit in the rod to the Kuhn length (see Fig. 7) |
| $\beta$ | $(k_BT)^{-1}$, $k_B$ and $T$ being the Boltzmann constant and temperature, respectively |
| $\eta$ | A dimensionless parameter introduced in Eq. (38) |
| $\kappa$ | Stiffness in the flexible rod model |
| $\psi$ | Helmholtz free energy of the individual chain |
| $\varepsilon$ | Required energy for liberation of one Kuhn segment in the rod |
| $\xi$ | A dimensionless parameter defined in Eq. (34) |
| $\xi_1$, $\xi_2$ | Dimensionless parameters defined in Eqs. (36a) and (36b) |
| $\zeta$ | The ratio of $a$ to the Kuhn length $b$ |

## 1. Introduction

To describe the mechanical properties of a wide range of synthetic polymers, such as rubber-like materials, it is conventional to model a uniform network containing the macromolecules as flexible chains connected together through covalent cross-linking (Treloar, 1975). However, studies reveal that the proposed strategy is inadequate for identifying the physical properties of many biopolymer gels (Clark and Ross-Murphy, 1985). In contrast to rubber-like materials, the constituting chains in many biopolymer gels randomly interlock with neighboring chains by means of physical rather than covalent cross-linking. The significance of such physical cross-linkages has been widely reported, for example in high strength hydrogels (Wang et al., 2017). As a result, models describing rubber elasticity encounter difficulties for capturing mechanical response of biopolymer gels. For example, the unorthodox relationship between the elastic moduli of Na- and Ca-alginate gels and the temperature can-

not be justified through a linear relationship predicted from the traditional rubber elasticity model (Moe et al., 1992). In addition, studies on biopolymer gels show that the thermal, mechanical, and chemical history of synthesis, including the type of polymer precursors, swelling/de-swelling, or heating/cooling gelation process, significantly affect the final properties of such gels. For instance, the mechanical features of Ca-alginate gels depend on the type of alginate and the preparation method (Moresi and Bruno, 2007).

Based on Clark and Ross-Murphy (1987), biopolymer gels are divided into two main groups: (i) rod-like ordered biopolymer gels such as globular proteins with branched networks where the pertinent networks are formed by junction points resembling synthetic polymers; (ii) disordered biopolymer gels such as polysaccharide gels in which the individual chains associate together laterally, forming helical junction zones and/or ion-mediated aggregation zones (egg-box structures) with length comparable to that of the coil parts of the chain. Figure 1 illustrates possible types of junction zones in disordered biopolymer networks. Compared with covalent bonds, the non-covalent links within the junction zones can more easily dissociate and re-associate. Consequently, when an external loading is applied, the junction zones can shrink by unwinding or expand by zipping, allowing the exchange of segments between the junction zone and coil region of the network. The rate of zipping/unzipping of the junction zones can be governed by several factors, including the concentration of cations or the temperature (Clark, 1991). Polymer networks such as gelatin or polysaccharide gels can therefore be envisaged as a collection of coil-rod structures serving as building blocks, where the rod and coil respectively represent the ordered junction zone and the remaining disordered region. For this reason, the elucidation of the mechanics of the coil-rod structure is of cardinal importance to gain insight into the properties of disordered

biopolymer networks.

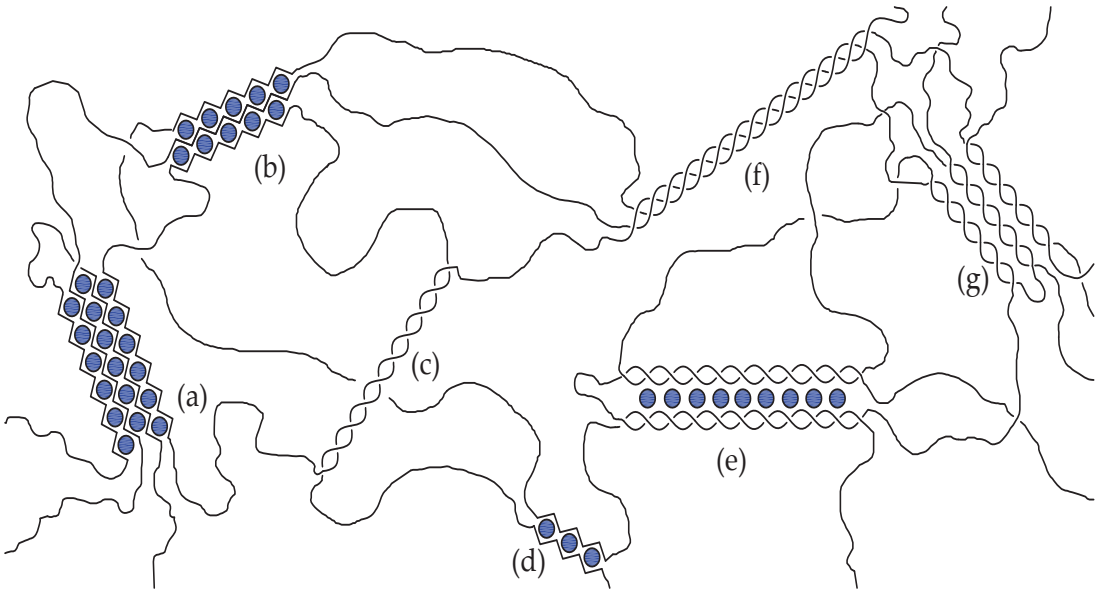


Figure 1: Examples of conformation and aggregation of junction zones in disordered biopolymer gel networks: (a)-(b) egg-box multimer (alginate), (c) double helix (agar), (d) egg-box dimer, (e) association of double helices with intermediate cations (carrageenan), (f) triple helix (gelatin), (g) association of double helices without intermediate cations (agarose gels). Each junction zone can be considered as a rod while the remaining disordered region can be considered as coils.

In the literature, there have been abundant studies that develop phenomenological models for the description of constitutive relations of biopolymer gels (McEvoy et al., 1985; Zhang et al., 2007; Clark and Ross-Murphy, 2009; Magnenet et al., 2012; Xu and Safran, 2015). Readers are referred to the comprehensive review of the continuum elastic models for biopolymer gels by Wang and Xu (2020). On the contrary, micro-mechanical studies accounting for behaviours at the molecular level are fairly limited. Some research focused on the constitutive relations of ordered biopolymer networks consisting of rod-like macromolecules. For

example, Doi and Kuzuu (1980) attempted to capture the energetic contribution of entanglements in such networks. Dobrynin and Carrillo (2011) proposed a micromechanical-based constitutive model capable of predicting the strain-hardening of synthetic polymer networks as well as ordered biopolymer gels such as actin. De Tommasi et al. (2015) adopted a multi-scale approach to derive a constitutive relationship for polymeric networks containing macromolecules with unfolding domains. Likewise, there is scant information on the micro-scale modelling of disordered biopolymer networks. Nishinari et al. (1985) proposed a reel model for the zipping/unzipping mechanism to explain the nonlinear effect of the temperature on the elastic modulus in thermoreversible gels. In their treatment, the junction zones served as a reservoir capable of changing the number of the Kuhn segments in the coils, although the junction zone itself was not explicitly incorporated in the formulation. Mechanics of the coil was described by the inverse Langevin model, with energy levels assigned to each conformation proportional to the number of Kuhn segments in the coil. This model was verified for different types of biopolymer gels (Nishinari, 2007). Inspired by this study, Higgs and Ball (1989) simplified the reel model using Gaussian approximation and obtained the partition function of a reel structure attached to a rigid rod with a fixed length. Subsequently, they studied the effects of the zipping mechanism by comparing the properties of the reel structure with the conventional coil structure. In their zipping/unzipping treatment, the total number of segments is not conserved as the length of the rod remains fixed while the number of Kuhn segments in the coil is allowed to change. In addition, a number of assumptions were made which led to some unphysical features such as discontinuity in the force-extension curve.

The main goal of this paper is to provide a comprehensive statistical mechanics frame-

work for modelling the coil-rod structure considering the exchange of segments between the disordered region (the coil) and the junction zone (the rod). Since the choice of ensemble depends on the question to be addressed and it can impact the results of the analysis, in section 2, the fundamental concepts behind different ensembles are clarified. Subsequently, in section 3, the statistical mechanics analysis of a rod structure is carried out with different ensembles. The formulation is extended to the coil-rod structure with fixed rod length in section 4, to derive the relationship between the force applied at the ends of the structure and the end-to-end separation. In section 5 the treatment of coil-rod structure is cast in a more general form to incorporate zipping and unzipping behaviour. Finally, as examples of its applications, in section 6 the model is implemented into the eight-chain model to describe the macroscopic mechanical response of a network, as well as used to predict the unwinding of a double-stranded DNA under a tensile force.

## 2. Statistical mechanics considerations of a macromolecule

The main focus of this work, which is a general interest for the study of macromolecules, is the relationship between the force applied at the two ends of the structure and the end-to-end extension. The theoretical assessment of this mechanical property necessitates the formulation of a partition function via statistical mechanics. Since the temperature, extension, applied force and number of units in the molecule are convenient measurable properties, we generally deal with three ensembles: Canonical ensemble, isothermal-isotension ensemble, and grand canonical ensemble.

*2.1. Canonical ensemble*

In the canonical ensemble, two possible scenarios can be considered:

(i) The structure is maintained at a fixed end-to-end position vector $\boldsymbol{r}$, fixed temperature $T$ and fixed number of segments $M$. An average force $\langle \boldsymbol{f}_r \rangle$ is required to maintain the structure with fixed end-to-end distance $|\boldsymbol{r}| = r$ along the direction $\frac{1}{r}\boldsymbol{r}$. If the canonical partition function $Z(\boldsymbol{r}, T, M)$ is at hand, one can derive a relationship between the $\langle \boldsymbol{f}_r \rangle$ and $\boldsymbol{r}$. For a single molecular structure, the direction of $\boldsymbol{r}$ is immaterial to the partition function $Z(\boldsymbol{r}, T, M)$. Thus, with no loss of generality, the end-to-end vector $\boldsymbol{r}$ can be replaced by "end-to-end distance $r$". The Helmholtz free energy $\psi$ is calculated from

$$\psi(r, T, M) = -\beta^{-1} \ln \left[ Z(r, T, M) \right], \tag{1}$$

in which $\beta = (k_B T)^{-1}$ and $k_B$ is the Boltzmann constant. The average force is colinear with the fixed end-to-end vector $\boldsymbol{r}$ and its magnitude $\langle f_r \rangle$ is calculated by

$$\langle f_r \rangle = \frac{\partial \psi(r, T, M)}{\partial r}. \tag{2}$$

This ensemble has been in the spotlight of abundant research due to its significance in incorporating the chain properties into a network. For instance, Higgs and Ball (1989) merely focused on canonical ensemble for the coil-rod structure.

(ii) The structure is kept at a fixed end-to-end "displacement", fixed temperature $T$ and fixed number of segments $M$. The displacement can be imposed in any arbitrary direction, while the other components of the end-to-end vector are free to move. Without loss of generality, we will call this arbitrary direction $x$ in this work. The average force

$\langle f_x \rangle$ required to keep the structure with fixed $x$ can be determined with the aid of this canonical ensemble, by recognizing that it is the work conjugate of $x$ and its direction is along the $x$ axis. Once the canonical partition function $Z(x, T, M)$ is available, the Helmholtz free energy is obtained as

$$\psi(x, T, M) = -\beta^{-1} \ln \left[ Z(x, T, M) \right]. \tag{3}$$

Now, by taking its derivative with respect to $x$, one can obtain the average force as

$$\langle f_x \rangle = \frac{\partial \psi(x, T, M)}{\partial x}. \tag{4}$$

Evidently, the number of conformations with fixed displacement is much larger than the previous ensemble. This stems from the fact that in the previous scenario, all displacement components $x$, $y$, and $z$ are fixed. Although studying scenario (i) is of more practical relevance, there is an interesting relationship between the two scenarios which facilitates the derivation of the partition function with fixed end-to-end distance. This relationship is established below.

Consider a chain with one end fixed at the origin and without any applied external forces. The probability that the other end of the chain is located in a volume element $\mathrm{d}\tau$ is given by (Flory, 1969)

$$W(\boldsymbol{r})\mathrm{d}\tau = \frac{Z\left(r, T, M\right) \mathrm{d}\tau}{Z_0}, \tag{5}$$

where

$$Z_0 = \int_{\tau} Z\left(r, T, M\right) \mathrm{d}\tau, \tag{6}$$

and $W(\boldsymbol{r})$ denotes the probability distribution as a function of $\boldsymbol{r}$, commonly referred to simply as the "distribution function". The volume element $\mathrm{d}\tau$ in (5) is located at the end of the position vector $\boldsymbol{r}$ with Cartesian coordinates $(x, y, z)$. Similar to $Z(\boldsymbol{r}, T, M)$, $W(\boldsymbol{r})$ depends on the end-to-end distance $r$ rather than end-to-end vector $\boldsymbol{r}$. Now, Eq. (1) is rewritten as

$$\psi(r, T, M) = -\beta^{-1} \ln\left[W(r)\right] + \text{cte}. \tag{7}$$

This alternative formulation enables us to use $W(r)$ to determine $\langle f_r \rangle$ vs. $r$ for the coil-rod structure. Likewise, if $p(x)\mathrm{d}x$ is the probability that one end of a structure, free of any external forces, is located between $x$ and $x + \mathrm{d}x$, while the other end is fixed at the origin, then:

$$p(x)\mathrm{d}x = \frac{Z\left(x, T, M\right)\mathrm{d}x}{\displaystyle\int_{x=-\infty}^{+\infty} Z\left(x, T, M\right)\mathrm{d}x}. \tag{8}$$

Fig. 2 depicts the aforementioned probabilities for the coil-rod structure with number of Kuhn segments $n$, Kuhn length $b$, and rod-length $a$. It can be readily shown that $W(r)$ and $p(x)$ satisfy the following equation:

$$-\left(\frac{\mathrm{d}p(x)}{\mathrm{d}x}\right)_{x=r} = 2\pi r W(r). \tag{9}$$

The detailed derivation of (9) is provided in Supplementary Information, Section S1. To emphasize that $W(r)$ and $p(x)$ are obtained in the absence of external forces, they are termed as the probability distribution of the "free" chains hereafter.

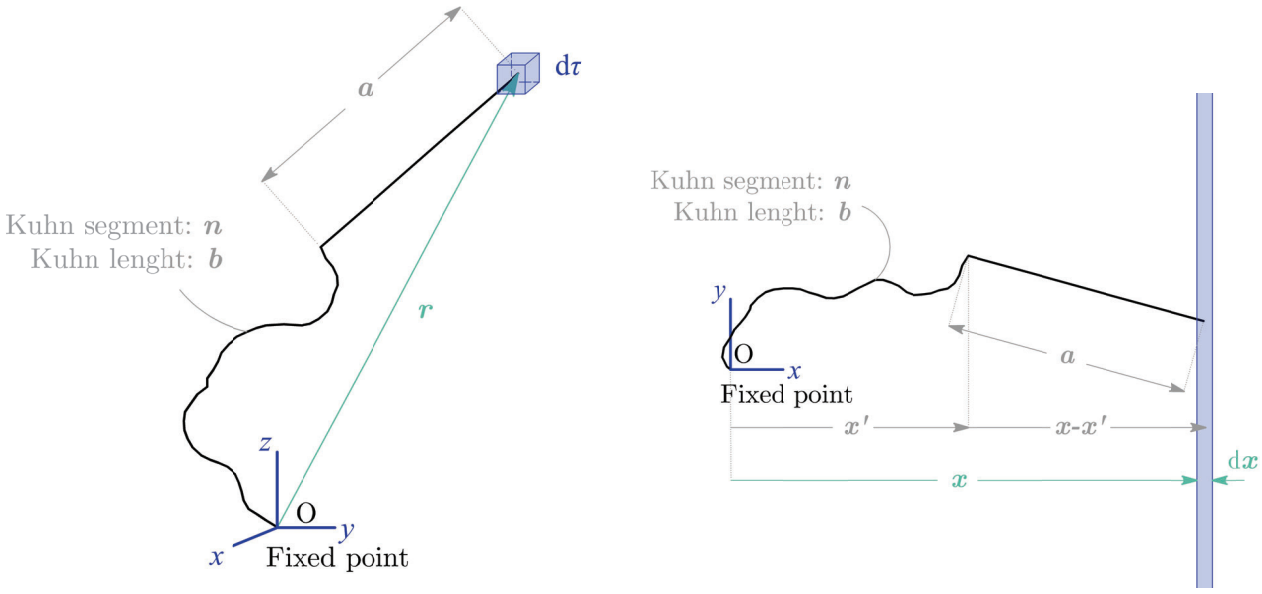


(a) Probability distribution $W_n^{\mathrm{CR}}(\boldsymbol{r})$ (b) Probability distribution $p_n^{\mathrm{CR}}(x)$

Figure 2: Schematics of the coil-rod structure and the two different probabilities. The superscript CR denotes the coil-rod structure, and the subscript $n$ indicates the number of Kuhn segments in the coil.

*2.2. Isothermal-isotension ensemble*

In this case, the structure with one fixed end is acted upon by a fixed force $\boldsymbol{f}$ at the other end under fixed temperature $T$ and a fixed number of segments $M$ (Flory, 1969)[1]. With no loss of generality, the coordinate system is set up such that $x$ axis is in the direction of the applied force and the magnitude of the force is designated by $f_x$. In this sense, different conformations with different $x$ can be established as a concomitant of the applied force. The average $\langle x \rangle$ is the work conjugate of the force $f_x$ and can be determined in the isothermal-isotension ensemble. Specifically, the isothermal-isotension partition function $Q(f_x, T, M)$ can be related to the canonical partition function $Z(x, T, M)$ by (Hill, 1986)

$$Q(f_x, T, M) = \frac{1}{\Delta l} \int_{-\infty}^{+\infty} Z(x, T, M) \exp\left[\beta f_x x\right] \mathrm{d}x, \tag{10}$$

where $\Delta l$ is a quantity with a dimension of length to ensure the dimensionless nature of the partition function. Because the derivation of the force-extension relationship involves differentiating the logarithm of the partition function, it is not influenced by the actual value of $\Delta l$. Alternatively, the isothermal-isotension partition function can be written in terms of $Z(r, T, M)$ by using spherical coordinates as below (Flory, 1969)

$$Q(f_x, T, M) = \frac{1}{\Delta l^3} \int_{\theta=0}^{2\pi} \int_{\phi=0}^{\pi} \int_{r=0}^{+\infty} Z(r, T, M) \exp\left[\beta f_x r \cos\phi\right] r^2 \sin\phi \, \mathrm{d}r \, \mathrm{d}\phi \, \mathrm{d}\theta. \tag{11}$$

After specification of $Q(f_x, T, M)$, the Gibbs free energy $G$ is derived as

$$G(f_x, T, M) = -\beta^{-1} \ln Q(f_x, T, M). \tag{12}$$

[1]This is analogous to the isothermal-isobaric ensemble for ideal gas with a fixed number of particles, fixed temperature $T$, and fixed applied pressure.

Subsequently,

$$\langle x \rangle = -\frac{\partial G(f_x, T, M)}{\partial f_x} \tag{13}$$

is utilized to obtain a relation between $\langle x \rangle$ and $f_x$.

### *2.3. Grand canonical ensemble*

In the ensembles discussed above, the length of the rod is considered fixed, which becomes inadequate if phenomena such as zipping and unzipping are to be accounted for. To allow for variable rod length and exchange of segments between the rod and coil portions of the structure, the grand canonical ensemble will be employed such that the structure is maintained at a fixed end-to-end position vector $\boldsymbol{r}$, fixed temperature $T$ and fixed chemical potential. This ensemble samples, according to the appropriate probability distribution, all possible conformations with different rod length or equivalently different number of Kuhn segments in the coil. The formulation in the grand canonical ensemble will be presented in section 5.

It should be acknowledged that there have been many discussions on the equivalence of ensembles in the thermodynamic limit which, in the context of chain mechanics, refers to $M \to \infty$. For the standard coil structure, different ensembles can lead to different results for small or moderate $M$ (Titantah et al., 1999), while convergence of different ensembles has been demonstrated for large $M$ (Winkler, 2010). The equivalence is no longer valid for certain polymer lattice models involving two equilibrium states for each segment. In this case, the force-extension relationships predicted from canonical and isothermal-isotension ensembles can be qualitatively different even for large $M$ (Giordano, 2018). The equivalence

of these two ensembles will be examined below for a single rod as well as for the coil-rod structure.

## 3. Analysis of a single rod

In this work, the junction zone is modeled as a single rigid rod. Different treatments are available in the literature. For example, in ordered biopolymer gels such as actin and collagen, the rod structures have been modeled using a semi-flexible chain with bending and axial stiffnesses (Carrillo et al., 2013). The worm-like chain model (Marko and Siggia, 1995) is another popular model often adopted for semi-flexible rod-like structures. The use of a non-deformable rod to represent the junction zone is a further simplification from the worm-like chain model, which is a reasonable assumption when the length of the rod is small compared to the persistence length of the worm-like chain (Buhot and Halperin, 2002). According to Weiner (Weiner, 1982), there are two distinct paths for the extraction of the partition function for a single rigid rod: (1) The rigid model in which the Hamiltonian of the rod is established based on the existing kinematic constraint. Hereafter, this model is referred to as Weiner's rigid model. (2) The flexible model in which the rod is first assumed to be flexible with a finite axial stiffness $\kappa$. Then, the result of a stiff rod is achieved by setting $\kappa$ to infinity. It should be noted that the term "flexible" for infinite $\kappa$ may be misleading as it represents the rigid rod structure *per se*; nevertheless, the results may be different from Weiner's rigid model. In the current section, the flexible model is examined in detail and the results from the canonical and isothermal-isotension ensembles are compared. The description of Weiner's rigid model is deferred to Supplementary Information Section S2 where the differences between the approaches are clarified.

Consider a segment AB placed between two fixed walls with distance $x$ at fixed temperature $T$ (see Fig. 3). The segment is modelled by a Hookean spring with stiffness $\kappa$ and unstretched length $a$. Furthermore, the mass $m$ of the segment is lumped at point B. Point A is affixed at the origin, while B is allowed to occupy any points on the right wall. Hence, the Hamiltonian of the segment is determined as

$$\mathscr{H} = \frac{1}{2m}(p_y^2 + p_z^2) + \frac{1}{2}\kappa\left(\sqrt{q_y^2 + q_z^2 + x^2} - a\right)^2. \tag{14}$$

In the above relation, $p_y$ and $p_z$ denote the components of the linear momentum of the concentrated mass $m$. $q_y$ and $q_z$ are the $y-$ and $z-$ components of the position vector of point B, respectively. Since the concentrated mass at B is confined to move in the $yz$ plane, the system has two degrees of freedom and the corresponding canonical ensemble partition function is

$$\begin{aligned} Z^{\mathrm{R}}(x,T) =& \frac{1}{h^2}\int_{p_y=-\infty}^{+\infty}\int_{p_z=-\infty}^{+\infty}\exp\left[-\frac{\beta}{2m}(p_y^2+p_z^2)\right]\mathrm{d}p_y\mathrm{d}p_z \\ &\times\int_{q_y=-\infty}^{+\infty}\int_{q_z=-\infty}^{+\infty}\exp\left[-\frac{\beta\kappa}{2}\left(\sqrt{q_y^2+q_z^2+x^2}-a\right)^2\right]\mathrm{d}q_y\mathrm{d}q_z, \end{aligned} \tag{15}$$

in which the Planck's constant $h$ is introduced to preserve the partition function dimensionless. In the above relation, superscript R is utilized to indicate the rod structure. After some mathematical manipulations, the above partition function is expressed as below:

$$Z^{\mathrm{R}}(x,T) = \frac{4\pi^2 m a^2}{\beta h^2}\left\{\frac{1}{\beta\kappa a^2}\exp\left[\frac{-\beta\kappa a^2}{2}\left(\frac{|x|}{a}-1\right)^2\right] + \sqrt{\frac{\pi}{2\beta\kappa a^2}}\,\mathrm{erfc}\left[\sqrt{\frac{\beta\kappa a^2}{2}}\left(\frac{|x|}{a}-1\right)\right]\right\}, \tag{16}$$

in which $\mathrm{erfc}\,(\cdots)$ signifies the complementary error function. In the limit of very large $\kappa$, one can obtain

$$Z^{\mathrm{R}}(x,T) = \sqrt{\frac{32\pi^5 m^2 a^2}{\beta^3 h^4}}\frac{H(x+a)-H(x-a)}{\sqrt{\kappa}}, \tag{17}$$

where $H(\cdots)$ is the Heaviside step function. By employing Eq. (17) in (8) it is found that

$$p^{\mathrm{R}}(x)\mathrm{d}x = \frac{\mathrm{d}x}{2a}\left(H(x+a) - H(x-a)\right). \tag{18}$$

which agrees with Treloar (1946) for a single rigid rod. Finally, by substituting Eq. (16) in (10), one can obtain the isothermal-isotension partition function as

$$Q^{\mathrm{R}}(f_x,T) = \frac{1}{\Delta l}\sqrt{\frac{8\pi^5 m^2}{\beta^5\kappa^3 h^4}}\frac{1}{\beta a f_x}\Bigg\{\exp\left[-\beta a f_x\left(1-\frac{\beta a f_x}{2\beta\kappa a^2}\right)\right]\left(\beta a f_x - \beta\kappa a^2\right)\left(1+\mathrm{erf}\left[\frac{\beta\kappa a^2-\beta a f_x}{\sqrt{2\beta\kappa a^2}}\right]\right) + \exp\left[\beta a f_x\left(1+\frac{\beta a f_x}{2\beta\kappa a^2}\right)\right]\left(\beta a f_x + \beta\kappa a^2\right)\left(1+\mathrm{erf}\left[\frac{\beta\kappa a^2+\beta a f_x}{\sqrt{2\beta\kappa a^2}}\right]\right)\Bigg\}, \tag{19}$$

in which $\mathrm{erf}(\cdots)$ represents the error function. For very large values of $\kappa$,

$$Q^{\mathrm{R}}(f_x,T) = \frac{1}{\Delta l}\sqrt{\frac{128\pi^5 m^2 a^4}{\beta^3\kappa h^4}}\frac{\sinh(\beta f_x a)}{\beta f_x a}, \tag{20}$$

which is equivalent to the well-known result of the partition function for a single segment of a freely jointed chain (Yamakawa, 1971).

After calculation of partition functions (16), the average applied force $\langle f_x\rangle$ can be obtained using Eqs. (3) and (4). In the normalized form,

$$\begin{aligned}\beta a\langle f_x\rangle &= \frac{2\beta\kappa a x}{2+\sqrt{2\pi\beta\kappa a^2}\exp\left[\frac{1}{2}\beta\kappa a^2\left(\frac{|x|}{a}-1\right)^2\right]\mathrm{erfc}\left[\sqrt{\frac{\beta\kappa a^2}{2}}\left(\frac{|x|}{a}-1\right)\right]} \\ &= \frac{2\beta\kappa a x}{2+\sqrt{2\pi\beta\kappa a^2}\exp\left[\frac{1}{2}\beta\kappa a^2\right]\left(1+\mathrm{erf}\left[\sqrt{\frac{\beta\kappa a^2}{2}}\right]\right)} + \mathscr{O}\left(\left(\frac{x}{a}\right)^2\right).\end{aligned} \tag{21}$$

The second step in Eq. (21) is obtained as a result of the Taylor expansion of the function about $x/a = 0$. Similarly, the average displacement $\langle x\rangle$ can be obtained in the isothermal-isotension ensemble by substituting (19) in Eqs. (12) and (13), which in the normalized form

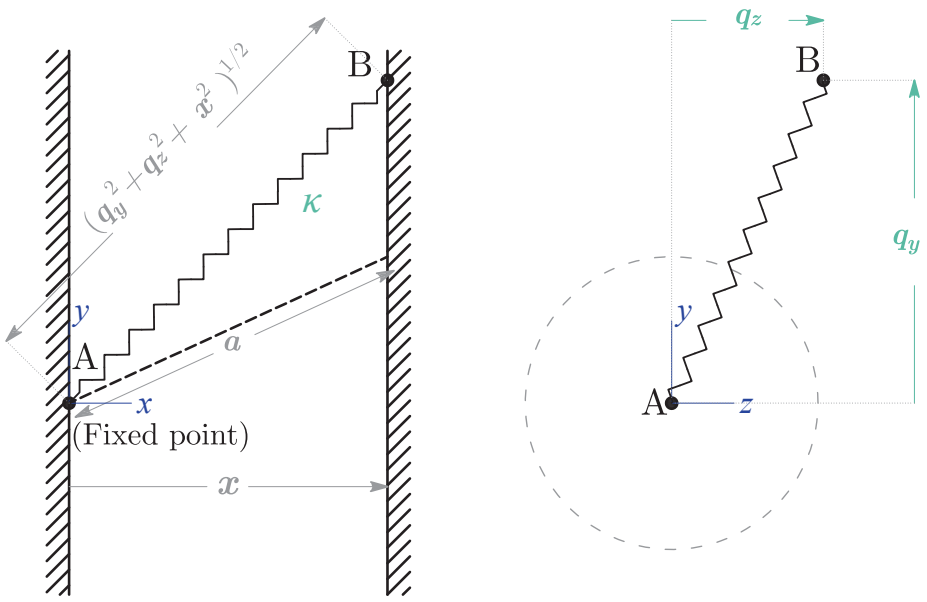


Figure 3: The single segment modelled by a Hookean spring is constrained between two fixed walls with a distance of $x$. Since the B end is allowed to occupy any position on the right wall, there are two degrees of freedom. The spring stiffness is $\kappa$ and the unstretched length of the segment is $a$.

is given by

$$\frac{\langle x\rangle}{a}=-\frac{1}{\beta a f_x}+\frac{1}{\beta\kappa a^2}\Bigg\{\sqrt{\frac{8(\kappa\beta a^2)^3}{\pi}}\exp\left[-\frac{\beta\kappa a^2}{2}\right]$$
$$+\exp\left[-\beta a f_x\left(1-\frac{\beta a f_x}{2\beta\kappa a^2}\right)\right]\left[\kappa\beta a^2+\left(f_x\beta a-\beta\kappa a^2\right)^2\right]\left(1+\operatorname{erf}\left[\frac{\beta\kappa a^2-\beta a f_x}{\sqrt{2\beta\kappa a^2}}\right]\right)$$
$$+\exp\left[\beta a f_x\left(1+\frac{\beta a f_x}{2\beta\kappa a^2}\right)\right]\left[\kappa\beta a^2+\left(f_x\beta a+\beta\kappa a^2\right)^2\right]\left(1+\operatorname{erf}\left[\frac{\beta\kappa a^2+\beta a f_x}{\sqrt{2\beta\kappa a^2}}\right]\right)\Bigg\}$$
$$\times\Bigg\{\exp\left[-\beta a f_x\left(1-\frac{\beta a f_x}{2\beta\kappa a^2}\right)\right]\left(\beta a f_x-\beta\kappa a^2\right)\left(1+\operatorname{erf}\left[\frac{\beta\kappa a^2-\beta a f_x}{\sqrt{2\beta\kappa a^2}}\right]\right)$$
$$+\exp\left[\beta a f_x\left(1+\frac{\beta a f_x}{2\beta\kappa a^2}\right)\right]\left(\beta a f_x+\beta\kappa a^2\right)\left(1+\operatorname{erf}\left[\frac{\beta\kappa a^2+\beta a f_x}{\sqrt{2\beta\kappa a^2}}\right]\right)\Bigg\}^{-1}. \tag{22}$$

For very large $\kappa$ the leading order term is

$$\frac{\langle x\rangle}{a}=\mathscr{L}\left(\beta a f_x\right)=\frac{1}{3}\beta a f_x+\mathscr{O}\left(\left(\beta a f_x\right)^3\right), \tag{23}$$

where $\mathscr{L}\left(\cdots\right)$ represents the Langevin function.

Fig. 4 shows the normalized force $\beta a\langle f_x\rangle$ versus $x/a$ obtained from the canonical ensemble for different values of $\beta\kappa a^2$. By increasing $\beta\kappa a^2$ the curves tend to level off for sufficiently small $x/a$ with a sharper increase toward infinity as $x$ approaches $a$. Fig. 4 also depicts the normalized applied force $\beta a f_x$ versus normalized average displacement $\langle x\rangle/a$ obtained from the isothermal-isotension ensemble for different values of $\beta\kappa a^2$. Clearly, for a given $\beta\kappa a^2$ this ensemble predicts stiffer behaviour compared to the canonical ensemble. The discrepancies between the two ensembles are negligible for $\beta\kappa a^2=1$, while larger differences between the ensembles are detected as $\beta\kappa a^2$ increases to 10000. This feature confirms that the rod structure cannot be considered as a macroscopic thermodynamic system.

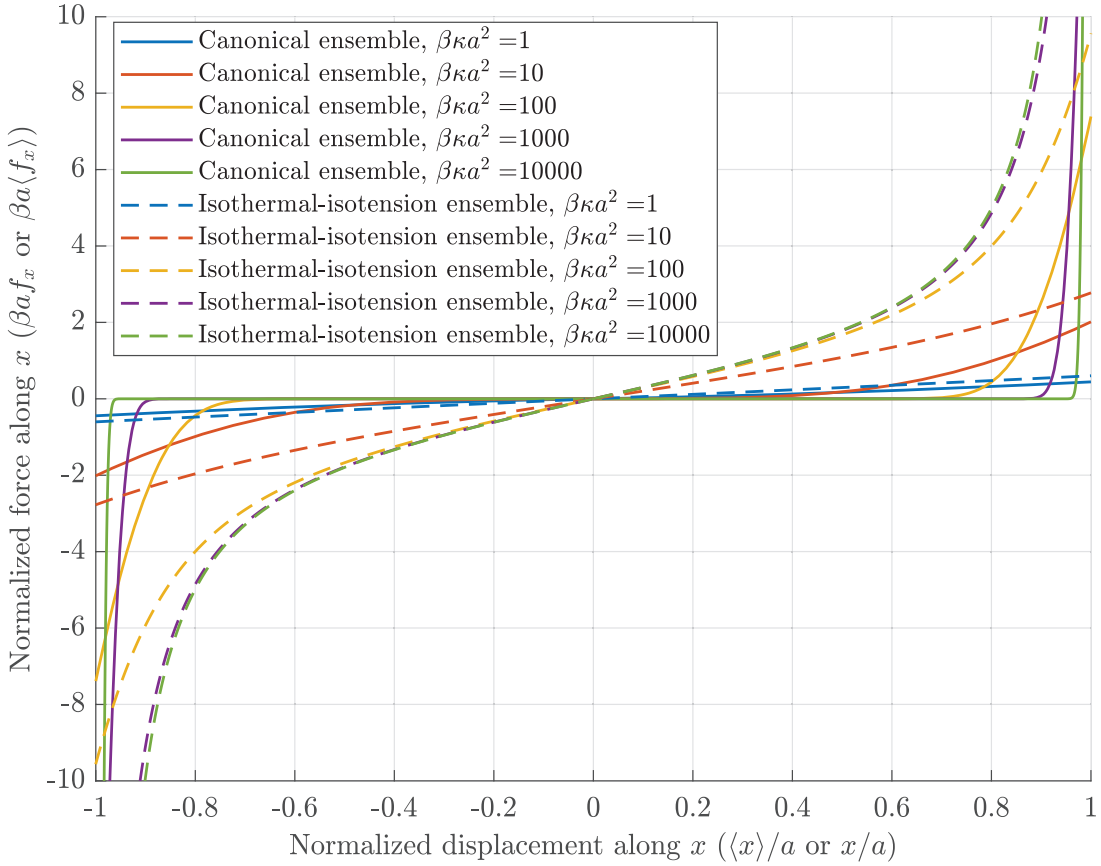


Figure 4: Normalized force vs. normalized displacement along the $x-$axis for different values of $\beta\kappa a^2$. For the isothermal-isotension ensemble $\beta a f_x$ is plotted against $\langle x\rangle/a$, while for the canonical ensemble $\beta a\langle f_x\rangle$ is plotted against $x/a$.

## 4. Coil-rod structure with fixed rod length

In this section, we will present the formulation for the determination of the force versus end-to-end distance (or $x$ displacement) of the coil-rod structure in the canonical and isothermal-isotension ensembles.

To calculate the probability distribution of the coil-rod structure $W_n^{\mathrm{CR}}(r)$, it is preferable to obtain the probability distribution along $x$ direction $p_n^{\mathrm{CR}}(x)$ in advance. Hereafter, the superscript CR indicates the coil-rod structure. For this purpose, it is convenient to employ

the convolution property to relate $p_n^{\mathrm{CR}}(x)$ to $p^{\mathrm{R}}(x)$ for the rod (Eq. (18)) and $p_n^{\mathrm{C}}(x)$ for the coil (see Fig. 2b):

$$p_n^{\mathrm{CR}}(x) = \int_{-\infty}^{+\infty} p_n^{\mathrm{C}}(x') p^{\mathrm{R}}(x - x') \mathrm{d}x' = \frac{1}{2a} \int_{x-a}^{x+a} p_n^{\mathrm{C}}(x') \mathrm{d}x'. \tag{24}$$

The latter identity is achieved through the use of Eq. (18). For the coil the superscript C has been added and the subscript $n$ is the number of Kuhn segments it contains. Carrying the above result into Eq. (9) and applying Leibniz integral rule yield

$$W_n^{\mathrm{CR}}(r) = \frac{1}{4\pi a r} \left[ p_n^{\mathrm{C}}(r - a) - p_n^{\mathrm{C}}(r + a) \right]. \tag{25}$$

Herein, without the explicit calculation of $W_n^{\mathrm{C}}(r)$ and $W^{\mathrm{R}}(r)$, the distribution function of the coil-rod structure $W_n^{\mathrm{CR}}(r)$ is achieved in terms of the probability distribution of the coil along $x$ direction, i.e., $p_n^{\mathrm{C}}(x)$.

### *4.1. Gaussian approximation*

Let us first approximate the coil structure by a Gaussian chain with Kuhn length $b$ and the number of Kuhn segment $n$. The probability $p_n^{\mathrm{C}}(x)$ of such structure is given by (Treloar, 1975)

$$p_n^{\mathrm{C}}(x) = \sqrt{\frac{3}{2\pi n b^2}} \exp\left[ -\frac{3x^2}{2nb^2} \right]. \tag{26}$$

Combining Eqs. (25) and (26) leads to

$$W_n^{\mathrm{CR}}(r) = \sqrt{\frac{3}{8n\pi^3 a^2 b^2}} \frac{1}{r} \exp\left[ -\frac{3}{2nb^2}(r^2 + a^2) \right] \sinh\left( \frac{3}{nb^2} ar \right), \tag{27}$$

which is equivalent to the model of Higgs and Ball (1989). It is important to note that the term "Gaussian distribution" only applies to the coiled part of the coil-rod structure, while

the coil-rod does not exhibit the Gaussian behaviour. By differentiating the Helmholtz free energy (7) with respect to $r$, the average external force $\langle f_r \rangle$ is derived as

$$a\beta\langle f_r\rangle = -\frac{3\zeta^2}{n}\mathscr{L}\left(\frac{3\zeta^2}{n}\,\frac{r}{a}\right) + \frac{3\zeta^2}{n}\left(\frac{r}{a}\right), \tag{28}$$

where $\zeta = a/b$. For small extension $r/a$, it can be readily shown that

$$a\beta\langle f_r\rangle = \frac{3\zeta^2}{n}\left(1 - \frac{\zeta^2}{n}\right)\frac{r}{a} + \mathscr{O}\left(\left(\frac{r}{a}\right)^2\right). \tag{29}$$

The above relation shows that the initial slope of the $\langle f_r\rangle - r$ curve is negative when $\zeta > \sqrt{n}$. This feature stems from the fact that under zero external force the coil structure has a maximum probability at zero end-to-end distance (see (26)), but the presence of the rod shifts the maximum of the probability (27) toward a non-zero end-to-end distance. Hereafter this distance will be denoted by $r^*$. It is worthwhile to mention that the above result is valid only if the number of Kuhn segments is large and the end-to-end distance of the coil is very small. In other words, the Gaussian description of the coil-rod structure is legitimate when $r \to a$ and $n \gg 1$. Performing Taylor series expansion of Eq. (28) about $r = a$, one can obtain an estimation of $r^*$ at which the average force $\langle f_r\rangle$ vanishes:

$$\frac{r^*}{a} \approx \frac{\mathscr{L}\left(\dfrac{3\zeta^2}{n}\right) - \dfrac{3\zeta^2}{n}\mathscr{L}'\left(\dfrac{3\zeta^2}{n}\right)}{1 - \dfrac{3\zeta^2}{n}\mathscr{L}'\left(\dfrac{3\zeta^2}{n}\right)}, \tag{30}$$

where $\mathscr{L}'(\cdots)$ is the first derivative of the Langevin function.

In the following, we provide a more rigorous calculation and the validity of the Gaussian approximation is inspected through comparison with the exact result.

*4.2. Exact treatment*

Compared to the coiled chain in rubber-like materials, the length of the coil between junction zones in biopolymers is not necessarily large. Therefore, the Gaussian distribution

assumption for the coil may be invalid, and it is necessary to account for the finite number of segments in the coil (McEvoy et al., 1985).

Consider a freely jointed chain with an arbitrary number of Kuhn segment $n$ subjected to no external force. If one end of this coil is located at the origin, the probability that the other end is located between $x$ and $x + \mathrm{d}x$, along an arbitrary direction $x$, is given by (Treloar, 1946)

$$p_n^{\mathrm{C}}(x)\mathrm{d}x = \frac{1}{2b}\sum_{s=0}^{k}\frac{n(-1)^s}{s!(n-s)!}\left[\frac{1}{2}\left(n-\frac{x}{b}\right)-s\right]^{n-1}\mathrm{d}x \quad \text{if } -(2k+2-n)b \le x \le (n-2k)b, \tag{31}$$

and zero for $|x| \ge nb$. In the above relation, $k = 0, 1, \cdots, n-1$. The substitution of Eq. (31) in Eq. (25) results in the exact form of $W_n^{\mathrm{CR}}(r)$, from which the average force can be determined:

$$a\beta\langle f_r\rangle = \frac{a}{r} - a\left(\frac{\mathrm{d}p_n^{\mathrm{C}}(r-a)}{\mathrm{d}r} - \frac{\mathrm{d}p_n^{\mathrm{C}}(r+a)}{\mathrm{d}r}\right)\left(p_n^{\mathrm{C}}(r-a) - p_n^{\mathrm{C}}(r+a)\right)^{-1}. \tag{32}$$

As a side note, in Supplementary Information Section S3, the closed-form expression of the probability distribution $p_n^{\mathrm{CR}}(x)$ is derived from (24) and (31).

### *4.3. Approximation for a large number of Kuhn segments*

As $x$ approaches $-nb$, the numerical calculation of summation in (31) for large $n$ encounters fluctuations. To circumvent this issue, we will devise an alternative remedy for large $n$. It should be emphasized that the Gaussian approximation in 4.1 is only valid if the end-to-end distance $r/b \ll 1$ and $n \gg 1$, while the current treatment is applicable for $n \gg 1$ irrespective of $r$ values.

The probability distribution of a freely jointed coil along $x$ direction can be expressed in a single term under certain conditions (Flory, 1969)[2],

$$p_n^{\mathrm{C}}(x) = \frac{A_0}{\sqrt{n}} \left[\frac{\sinh\xi}{\xi}\right]^n \exp\left[-\frac{\xi x}{b}\right], \tag{33}$$

in which

$$\xi = \mathscr{L}^{-1}\left(\frac{x}{nb}\right), \tag{34}$$

and $A_0$ is a normalization factor and a function of $b$. Substituting (33) into Eq. (25) yields

$$W_n^{\mathrm{CR}}(r) = \frac{A_0}{4\pi a r\sqrt{n}} \left\{ \left[\frac{\sinh\xi_1}{\xi_1}\right]^n \exp\left[-\xi_1\zeta\left(\frac{r}{a}-1\right)\right] - \left[\frac{\sinh\xi_2}{\xi_2}\right]^n \exp\left[-\xi_2\zeta\left(\frac{r}{a}+1\right)\right] \right\}, \tag{35}$$

in which

$$\xi_1 = \mathscr{L}^{-1}\left[\frac{\zeta}{n}\left(\frac{r}{a}-1\right)\right], \tag{36a}$$

$$\xi_2 = \mathscr{L}^{-1}\left[\frac{\zeta}{n}\left(\frac{r}{a}+1\right)\right]. \tag{36b}$$

The average force applied at the ends of the coil-rod structure can therefore be calculated from the Helmholtz free energy,

$$a\beta\langle f_r\rangle = \frac{a}{r} + \zeta \frac{\xi_1 \left[\frac{\sinh\xi_1}{\xi_1}\right]^n \exp\left[-\xi_1\zeta\left(\frac{r}{a}-1\right)\right] - \xi_2 \left[\frac{\sinh\xi_2}{\xi_2}\right]^n \exp\left[-\xi_2\zeta\left(\frac{r}{a}+1\right)\right]}{\left[\frac{\sinh\xi_1}{\xi_1}\right]^n \exp\left[-\xi_1\zeta\left(\frac{r}{a}-1\right)\right] - \left[\frac{\sinh\xi_2}{\xi_2}\right]^n \exp\left[-\xi_2\zeta\left(\frac{r}{a}+1\right)\right]}. \tag{37}$$

For small values of $r/a$, and $a < nb$ ($\zeta < n$) it can be shown that

$$a\beta\langle f_r\rangle = \zeta^2 \frac{3 - n\eta^2\mathscr{L}'(\eta)}{3n\mathscr{L}'(\eta)} \frac{r}{a} + \mathscr{O}\left(\left(\frac{r}{a}\right)^2\right), \tag{38}$$

[2]These conditions are thoroughly discussed in Flory's book. During the derivation, the summation of probabilities in (31) is replaced by an approximate expression, and then the factorial functions are estimated with Stirling's approximation.

where $\eta = \mathscr{L}^{-1}\left(\frac{\zeta}{n}\right)$. For large $n$ the result of the Gaussian approximation (29) can be recovered from Eq. (38).

*4.4. Comparison of different results in the canonical ensemble*

The normalized average force $\beta a\langle f_r\rangle$ is plotted against the normalized end-to-end distance $r/a$ for fixed $\zeta = 5$ and $n = 5$, 10, 25 in Fig. 5. Three cases are considered below and the results are provided for the exact model (32), Gaussian approximation (28), and large $n$ approximation (37).

*Case 1:* $\zeta^2 \leq n$

Demonstrated by the curves with $n = 25$ in Fig. 5, the coil component in this case is dominant, and hence the behaviour of the curves resembles that of coiled chains without a rod component. The average force monotonically increases as the structure extends. The Gaussian and large $n$ approximations both have reasonable agreement with the exact model for small $r/a$. For $r/a > 2.5$ the large $n$ approximation still agrees well with the exact model, while there is a substantial deviation from the Gaussian approximation. This is due to the assumption of small end-to-end distance for the coiled structure inherited from the Gaussian approximation.

*Case 2:* $\zeta < n < \zeta^2$

As shown in Fig. 5, for $n = 10$ there are two states with zero force, at $r = 0$ and $r^* = 0.83a$. Recall that $r^*$ represents the end-to-end distance with maximum probability. In this case, the curves behave completely differently from the conventional force-extension curves in that a convexity appears in the plots. The convex behaviour reflects the fact that the maximum

probability of the free coil-rod structure occurs at a non-zero end-to-end distance ($r^*$) as opposed to zero in the pure free coil chain model. For this reason, such a structure can sustain compressive forces if $r < r^*$. Physically, the phenomenon is caused by the presence of the rod, which has a rigid structure and when its length is comparable to the contour length of the coil, a compressive force is required to reach sufficiently small end-to-end distance for the coil-rod structure. The zero end-to-end distance $r = 0$ still represents an equilibrium state, albeit unstable. Similar to the previous case, the large $n$ approximation agrees with the exact model for the entire range of $r$, while the Gaussian approximation departs from the exact model significantly as the end-to-end distance increases. In particular, under the Gaussian approximation, the coil-rod structure is permitted to be stretched more than its contour length, i.e., $r/a = 3$, which is not realistic within the framework of entropic elasticity.

*Case 3:* $\zeta \geq n$

For this case, the length of the rod is greater than the contour length of the coil, i.e., $nb < a$, and it is impossible to reach zero end-to-end distance. This feature can be captured by the curves in Fig. 5 with $n = 5$ (exact result and large $n$ approximation) in which infinite compressive force is required to push the two ends toward each other. Zero force is found to occur at $r^* = 0.92a$ which is the end-to-end distance with the highest probability of the free coil-rod structure. Clearly, the curve predicted from the Gaussian approximation differs drastically from the other two curves not only for large extension $r/a > 1.5$ but also for small extension $r/a < 0.5$. Such a poor performance of the Gaussian approximation is expected and necessitates the application of the non-Gaussian model for smaller $n$ or large $a$.

It is worthwhile to mention that in all cases, the average force predicted from the exact

model goes to infinity as the end-to-end distance approach the fully stretched state, i.e., $r \to a + nb$. Moreover, as $r/a$ approaches 1, the accuracy of the Gaussian approximation increases because of the small extension of the coil.

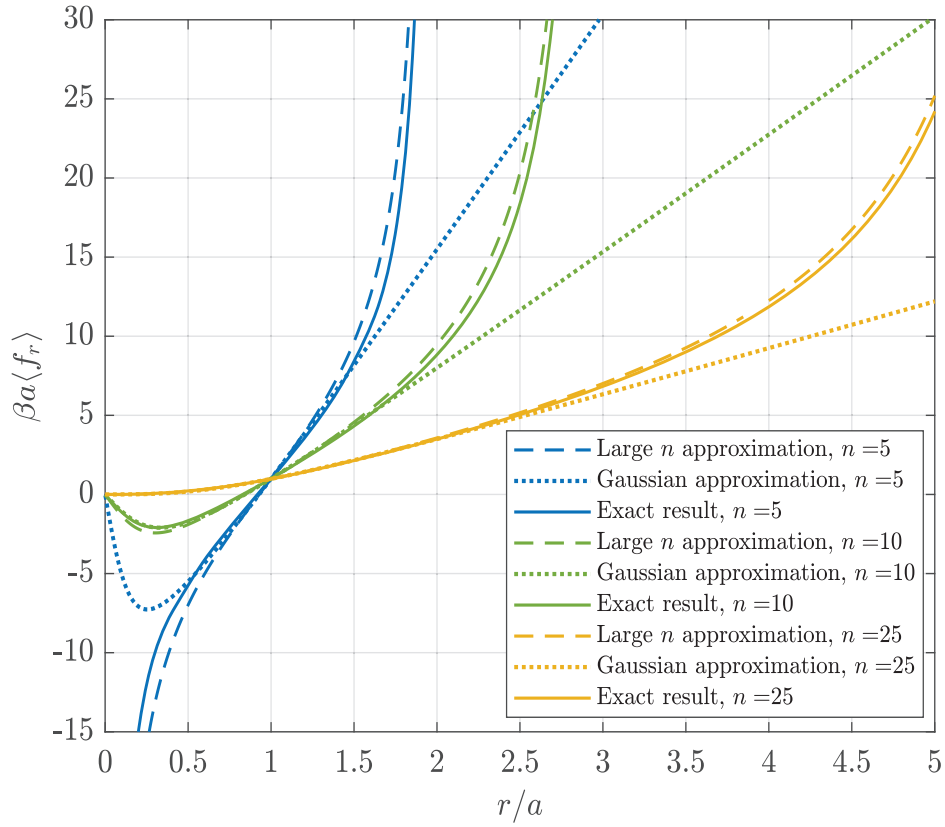


Figure 5: Normalized force $\beta a\langle f_r\rangle$ vs. normalized end-to-end distance $r/a$ of the coil-rod structure with fixed $\zeta = 5$ and Kuhn segments $n = 5$, 10, 25 in the coil.

### *4.5. Comparison between canonical and isothermal-isotension ensembles*

When an applied force is prescribed in $x-$direction, the coil-rod structure can take different conformations with various end-to-end vectors $\boldsymbol{r}$. The exact canonical partition function has been obtained via Eqs. (25), (31), and (5). By substituting the result in (11) it can be

shown that

$$Q(f_x, T, n+1) = Z_0 \frac{4\pi \sinh\left(f_x \beta a\right)}{f_x \beta a} \left( \frac{4\pi \sinh\left(f_x \beta b\right)}{f_x \beta b} \right)^n . \tag{39}$$

Now, by utilizing Eq. (13), we have

$$\frac{\langle x \rangle}{a} = \mathscr{L}\left(f_x \beta a\right) + \frac{nb}{a} \mathscr{L}\left(f_x \beta b\right) = \frac{1}{3} \beta a f_x \left[ 1 + \frac{n}{\zeta^2} \right] + \mathscr{O}\left( \left(f_x \beta a\right)^2 \right). \tag{40}$$

The second step of the above equation shows the asymptotic behaviour of the function near the origin. The normalized value of $\beta a f_x$ is depicted versus $\langle x \rangle / a$ in Fig. 6 for $\zeta = 5$ and different $n = 5,\ 10,\ 15$. By increasing $n$ the curves tend to behave more linearly, and the Gaussian characteristics of the coil-rod structure are more pronounced. Fig. 6 also shows the results from the canonical ensemble in dashed lines, which are obtained by applying Eqs. (S19) and (8) in (3) and (4). Although one ensemble measures the average of the displacement $\langle x \rangle$ and the other measures the average of the applied force $\langle f_x \rangle$, good agreement between the two ensembles is observed. The results at small $x$ are still distinguishable due to the presence of the rod structure mentioned in section 3, but the discrepancies fade away as $x$ increases. One feature of the $f_x$ (or $\langle f_x \rangle$) vs. $\langle x \rangle$ (or $x$) is that the initial slope is always positive, which is different from the $\langle f_r \rangle$ vs. $r$ result derived from the canonical ensemble (Fig. 5). In fact, for canonical ensemble with prescribed displacement $x$, even for very small $x$, the coil-rod structure can still access conformations with large end-to-end distance $r$ due to the displacements along $y$ and $z$ directions. Consequently, a compressive force is not required to maintain a small displacement $x$ as opposed to the case with a small end-to-end distance $r$.

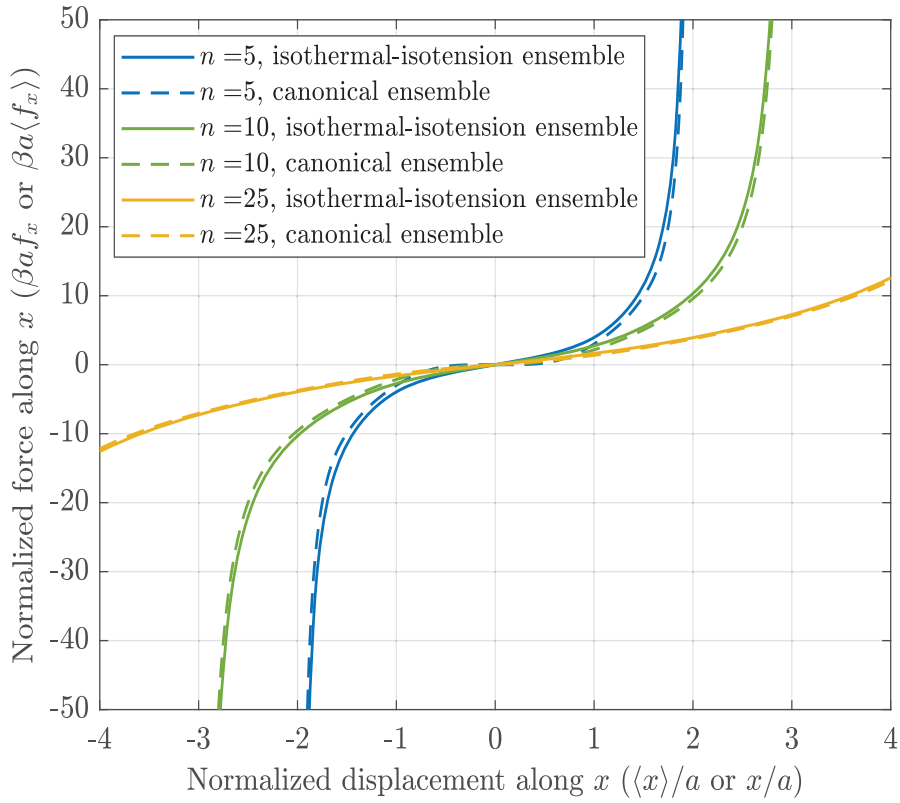


Figure 6: Normalized force vs. normalized displacement along $x$ direction for $\zeta = 5$ and $n = 5,\ 10,\ 25$. For the isothermal-isotension ensemble $\beta a f_x$ is plotted against $\langle x \rangle / a$, while for the canonical ensemble $\beta a \langle f_x \rangle$ is plotted against $x/a$.

## 5. Coil-rod structure with zipping/unzipping mechanism

As it was alluded to, external mechanical loading may cause the unzipping of the segments contributing to the junction zones. For example, in ion-mediated biopolymers, the trapped cations are set free from the junction zones under the external loading, and the length of the associated junction zones is reduced accordingly. To incorporate the zipping/unzipping mechanism, the Boltzmann average of statistical mechanics will be used. This treatment considers each coil-rod conformation with a different rod length as an equilibrium point in

the phase space. The energy of each conformation is ascertained based on the binding energy of the constituent units of the rod. As the number of these units increases, the total energy of the coil-rod structure decreases and the structure tends to be more stable. The number of Kuhn segments in the coil is reduced during the formation of new units in the rod. If we suppose that $N$ is the number of Kuhn segments in the completely unwound system (purely coiled structure), then the number of Kuhn segments participating in the rod is $N - n$. Without loss of generality, we define an effective unit in the rod such that it is formed from one Kuhn segment from the coil. The number of effective units in the rod is therefore $N-n$. The length of each effective unit is denoted by $\alpha b$ with $\alpha$ being the ratio between the length of one unit in the rod and the Kuhn length. Accordingly, the length of the rod $a$ is dependent on $n$ as below

$$a = (N - n)\alpha b. \tag{41}$$

We denote the energy required to liberate one effective unit from the rod by $\varepsilon$. Fig. 7 illustrates the energy landscape of the rod, using the egg-box model as an example. As $n$ increases and the effective units are released from the rod, the energy of the rod increases, reaching different equilibrium states (energy wells) separated by multiple of $\varepsilon$. The length $\alpha b$ is also shown in the rod structure.

By applying the Boltzmann average and Eq. (5), one can write the partition function for a coil-rod with prescribed end-to-end vector $\boldsymbol{r}$ but variable $n$,

$$\Omega(\boldsymbol{r}, T, \varepsilon) = Z_0 \exp\left[\beta N \varepsilon\right] \sum_{n=n_{\min}}^{n_{\max}} W_n^{\mathrm{CR}}(\boldsymbol{r}) \exp\left[-\beta n \varepsilon\right], \tag{42}$$

where $n_{\min}$ and $n_{\max}$ are respectively the minimum and maximum allowable numbers of Kuhn segments in the coil during zipping/unzipping. This form is equivalent to the grand

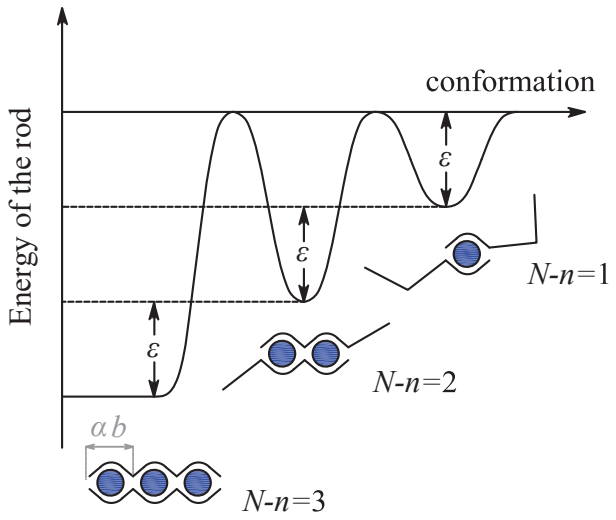


Figure 7: Schematics representation of the energy landscape for the rod, using egg-box model for illustration.

canonical partition function with fixed chemical potential $\varepsilon$. Let us rewrite Eq.(42) as

$$\Omega(r,T,\varepsilon) = Z_0 \exp\left[\beta N \varepsilon\right] \sum_{n=n_{\min}}^{n_{\max}} \exp\left\{\ln\left[W_n^{\mathrm{CR}}(r)\right] - n\beta\varepsilon\right\}, \tag{43}$$

where the vector $\boldsymbol{r}$ has been replaced by $r$ due to the dependence of $W_n^{\mathrm{CR}}(\boldsymbol{r})$ through $r$. At fixed $r$, by increasing $n$ the probability distribution $W_n^{\mathrm{CR}}(r)$ increases as a result of having more conformations. On the other hand, the energy level goes up due to the liberation of the units from the rod. These two competing effects can yield a specific value of $n_0(r)$ for which the argument of the exponential function in (43) is maximum. This term makes the most contribution to the sum in (43), and examination of the variation of $n_0$ with respect to $r$ allows us to detect the occurrence of zipping/unzipping. Specifically, a flat region of $n_0$ vs. $r$ indicates the tendency of the structure to have a fixed number of Kuhn segments in the coil, while a region of varying $n_0$ vs. $r$ shows the tendency of the structure to update the number of Kuhn segments through zipping or unzipping processes. After the calculation of

$\Omega(r, T, \varepsilon)$ in Eq. (43), the grand canonical potential can be determined as

$$\Phi(r, T, \varepsilon) = -\beta^{-1} \ln \left[\Omega(r, T, \varepsilon)\right], \tag{44}$$

from which the average force is evaluated by

$$\langle f_r \rangle = \frac{\partial \Phi(r, T, \varepsilon)}{\partial r}. \tag{45}$$

Fig. 8a shows the normalized force $\beta b \langle f_r \rangle$ vs. the normalized end-to-end distance $r/b$ for $N = 20$, $n_{\min} = 5$, $n_{\max} = 19$, $\alpha = 0.8$ and $\varepsilon\beta = 0.1$. Here the large $n$ approximation for $W_n^{\mathrm{CR}}(\boldsymbol{r})$ (Eq. (35)) has been used to ensure numerical stability. Results for fixed $n$ at $n_{\min}$ and at $n_{\max}$ are also plotted for comparison. The inset shows the variation of $n_0$ with $r/b$. A qualitative comparison of the main plot with the inset identifies five different regimes. For $r/b \leq 2$, the structure has a fixed number of Kuhn segments, $n_0$ is constant and the force-extension curve converges to that of the coil-rod structure with fixed $n = 19$. For $2 \leq r/b \leq 11.7$, $n_0$ decreases with $r/b$ suggesting the occurrence of zipping. The force-extension relationship starts deviating from the curve that corresponds to $n = 19$ and moving towards the curve that corresponds to $n = 5$. Meanwhile the plot exhibits negligible average force and hence stiffness. In other words, when the applied force is small, the coil-rod structure is able to achieve different end-to-end distances by varying the number of units in the rod. For $11.7 \leq r/b \leq 16.7$, $n_0$ is constant again, and the force-extension curve almost overlaps with the curve corresponding to fixed $n = 5$. With this maximum rod length, the structure can bear the normalized tensile force up to 17. In the regime of $16.7 \leq r/b \leq 18.4$, $n_0$ increases with $r/b$ indicating the unwinding of the coil-rod structure and its transition towards $n = 19$. The unwinding alleviates the loading on the structure and a slightly decreasing trend is observed in the force-extension curve. It should be noted that some

small fluctuations exist in the curve in this regime, which is not due to the numerical issues. Rather, this is caused by the discrete nature of $n$ in the summation (43). In other words, each oscillation in the curve corresponds to, on average, the liberation of one unit from the rod. Finally, when $r/b \geq 18.4$, $n_0$ stays at 19 and the load-bearing nature of the structure is activated, with sharp increase in the normalized force at the minimum rod length.

To demonstrate the effects of binding energy, Fig. 8b shows the results under the same condition as in Fig. 8a except for a larger binding energy of $\varepsilon\beta = 5$. A close examination of the main curve with the inset shows the presence of four regimes. When $r/b \leq 8.3$, $n_0$ decreases with $r/b$ and zipping occurs. Unlike in Fig. 8a, at $r/b = 0$, $n_0 = 10$ instead of $n_{\max} = 19$ and its decreasing trend starts immediately after $r/b$ deviates from zero. This distinct feature is caused by the larger binding energy, which drives the units to zip and form the rod. The force-extension curve is substantially different from both reference curves (corresponding to $n = 19$ and 5) in this regime. Notably, the force is compressive, this can be explained by the lengthening of the rod and shortening of the coil part which tend to generate a bulkier structure. A similar observation is made in Fig. 5 where short coil require compressive force to achieve a small end-to-end distance. For $8.3 \leq r/b \leq 16.9$, $n_0$ is at $n_{\min} = 5$ and the force-extension curve also agrees with the one at maximum rod length. In addition, the force transitions from compression to tension at $r/b = 11.8$. Further extension causes unzipping in the range of $16.9 \leq r/b \leq 19.4$. Similar to Fig. 8a, upon unzipping the force shows an overall decreasing trend, but the oscillations in the curve are much more pronounced because the liberation of one unit from the rod is associated with more substantial change in the energy. Beyond $r/b \geq 19.4$, the rod reaches its minimum length and the force on the structure increases significantly with the end-to-end distance. It

is worth pointing out that in the formulation of zipping/unzipping, $\beta$ and $\varepsilon$ always appear together as the product $\beta\varepsilon$. Therefore, increasing the binding energy $\varepsilon$ is equivalent to increasing $\beta$ or decreasing the temperature. The comparison between Fig. 8a and Fig. 8b hence also demonstrates the change in the behaviour of the coil-rod structure caused by decreasing the temperature. Figs. 8a and 8b also remove the discontinuity that appeared in the force vs. extension curve obtained by Higgs and Ball (1989). The discontinuity was caused by a number of assumptions in their partition function calculation which are avoided in the current work.

## 6. Demonstration of model application

### *6.1. Implementation in eight-chain model*

In this section, the force-extension relationship developed in this work is implemented into the macroscopic eight-chain model of Arruda and Boyce (1993) to predict the mechanical response of a network containing coil-rod structures. Following the idea of Arruda and Boyce (1993), eight coil-rod structures are placed in a cube such that for each structure, one of its ends is fixed at the center while the other is tethered at a corner of the cube. The Helmholtz free energy per unit reference volume can be written in terms of the end-to-end distance of the chain $r_{\text{chain}}$ in the current configuration

$$\Psi = \sum_{i=1}^{\mathscr{N}} \psi_i(r_{\text{chain}}), \tag{46}$$

where $\mathscr{N}$ refers to the number of chains per unit reference volume. $\psi_i$ is the energy stored in the $i$th chain

$$\psi_i(r_{\text{chain}}) = \int_{r_0}^{r_{\text{chain}}} \langle f_r \rangle \, \mathrm{d}r, \tag{47}$$

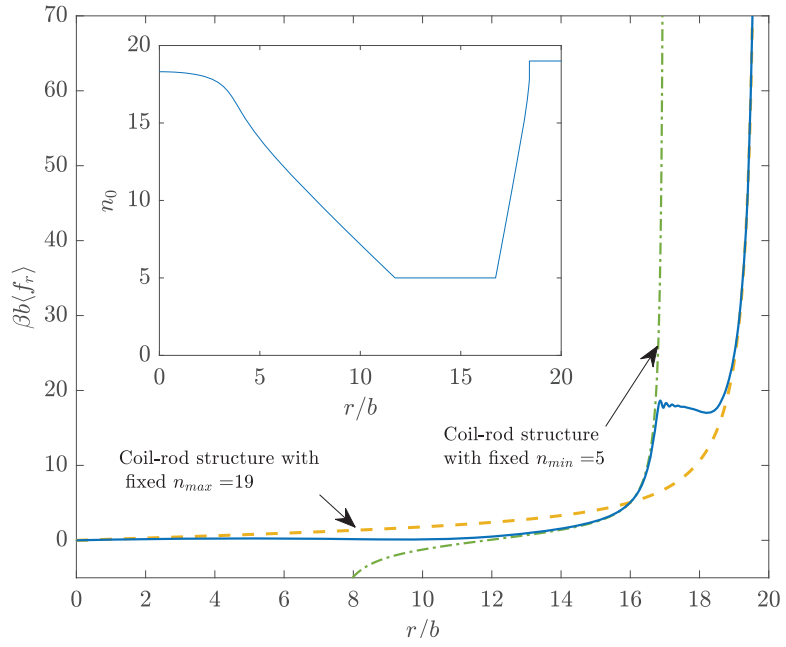


(a)

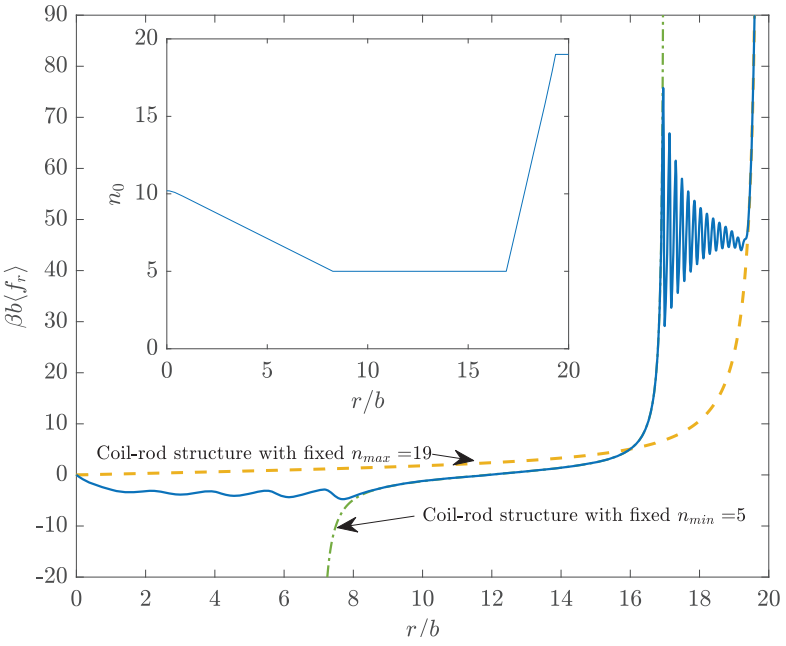


(b)

Figure 8: Normalized force $\beta b\langle f_r\rangle$ vs. normalized end-to-end displacement $r/b$ of the coil-rod structure for $\varepsilon\beta = 0.1$ in (a) and 5 in (b). The insets show the associated value of $n_0$ against $r/b$. The results are produced with $N = 20$, $n_{\max} = 19$, $n_{\min} = 5$, and $\alpha = 0.8$.

where $r_0$ is the end-to-end distance of the chain in the reference configuration. If the cube edges are parallel to the principal stretches $\lambda_1$, $\lambda_2$, and $\lambda_3$, it can be shown that the end-to-end distance of each chain in the current configuration $r_{\text{chain}}$ is given as (Arruda and Boyce, 1993):

$$r_{\text{chain}} = \frac{r_0}{\sqrt{3}} \left(\lambda_1^2 + \lambda_2^2 + \lambda_3^2\right)^{1/2}. \tag{48}$$

Differentiating (46) while assuming all chains to be identical and imposing incompressibility $\lambda_1\lambda_2\lambda_3 = 1$, the principal Cauchy stresses ($\sigma_i$, $i = 1, 2, 3$) can be obtained

$$\sigma_i = \lambda_i \frac{\mathrm{d}\Psi}{\mathrm{d}\lambda_i} + p_0 = \frac{\mathscr{N} r_0 \lambda_i^2}{\sqrt{3}\left(\lambda_1^2 + \lambda_2^2 + \lambda_3^2\right)^{1/2}} \langle f_r \rangle \Big|_{r_{\text{chain}}} + p_0, \tag{49}$$

where $p_0$ is the unknown pressure to be determined from the boundary conditions. Clearly, the stress-stretch relations directly depend on the force-extension behaviour of the constituent chains, i.e., $\langle f_r \rangle$-$r$ . For coil-rod structures with fixed rod and coil lengths, $\langle f_r \rangle$ can be obtained via Eqs. (28), (32), or (37) for various approximations. It should be noted that the end-to-end distance $r_0$ in the reference configuration is taken to be $\sqrt{n}b$ for a freely jointed chain (Treloar, 1975), which is not applicable for the coil-rod structure. Instead, we determine $r_0$ from

$$r_0 = \int_0^\infty r W_n^{\text{CR}}(r) \mathrm{d}r, \tag{50}$$

which is the average end-to-end distance of a coil-rod structure subjected to zero force. Fig. 9 shows the normalized principal stress $\sigma_1/\mu$ ($\mu = \mathscr{N}\beta^{-1}$) vs. the principal stretch $\lambda_1$ for three different loading conditions: biaxial (with equal stretches in directions 1 and 2), uniaxial (stretch in direction 1) and pure shear (in the 1-2 plane). $\langle f_r \rangle$-$r$ relation in Eq. (37) is used for $n = 25$ and different $\zeta = 0$, 5, 25. $\zeta = 0$ corresponds to the case where

the rod is absent and the coil-rod structure reduces to a freely jointed chain. For any given loading condition, as the length of the rod increases, the network becomes stiffer and the difference can be significant. For instance, by introducing a rod with the length equal to 5 Kuhn segments, $\sigma_1$ is doubled at $\lambda_1 = 3$ for uniaxial tension and pure shear, and more than doubled for biaxial loading. This signifies the importance of considering the rod element in macroscopic modeling of biopolymer gel networks.

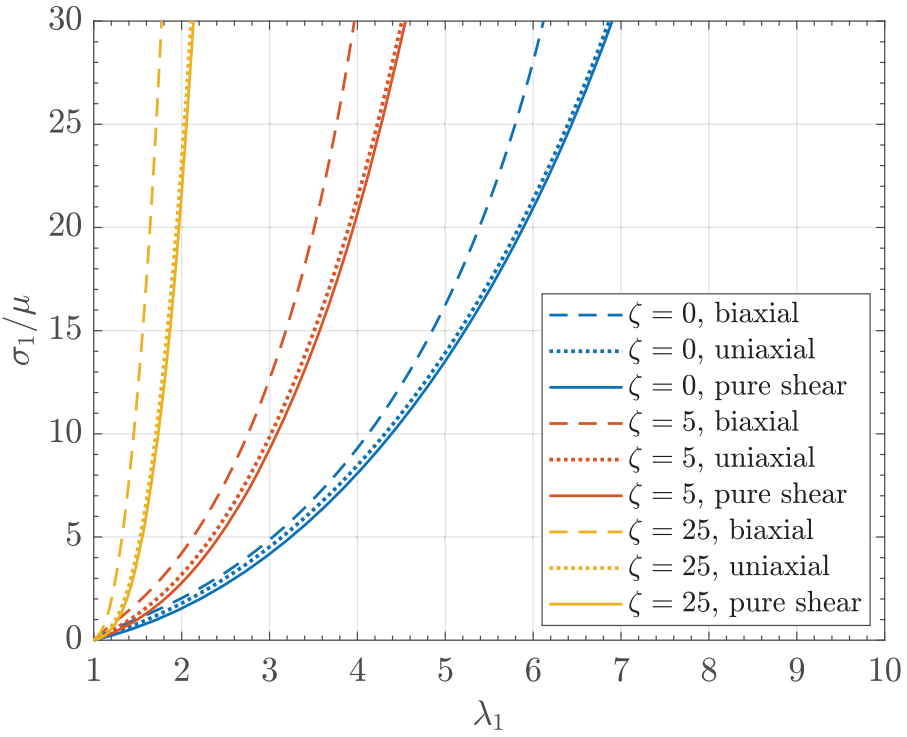


Figure 9: Normalized Cauchy stress $\sigma_1/\mu$ vs. the principal stretch $\lambda_1$ for biaxial, uniaxial and pure shear loadings of a biopolymer gel network modeled by implementing Eq. (37) into the eight-chain model of Arruda and Boyce (1993). The coil has a fixed number of Kuhn segments $n = 25$, while different rod lengths are considered, $\zeta = 0$, 5, 25.

*6.2. Prediction of DNA unwinding*

In this section, we test the validity of the proposed zipping/unzipping mechanism against existing experimental data. For this purpose, the experiments performed by Clausen-Schaumann et al. (2000) are considered, which involve the unwinding of a double-stranded DNA. The exploration of DNA unwinding is crucial as it occurs extensively in biological processes, including replication, transcription and DNA-protein interaction (Liebl and Zacharias, 2017). Clausen-Schaumann et al. (2000) reported the stretching of a 1.5 $\mu$m-long segment of double-stranded $\lambda$-BstE II digest DNA at $T = 20°$C using atomic force microscopy (AFM). They observed that after a highly cooperative mechanism, a conformational transition occurred at force 65 pN. At this point, the DNA double helix started to shrink, and only one of the two strands remained attached to the AFM tip and to the substrate. Below we show that the current model is capable of capturing the unwinding process and the conversion of the double-stranded DNA to single-stranded ones. Here, the double-stranded DNA is modelled as the rigid rod, while the single-stranded DNA is treated as a freely jointed coil structure. Under applied loading, the double-stranded DNA unwinds completely so that $N = n_{\max}$, and the number of unknown parameters in the model reduces to $n_{\min}$, $n_{\max}$, $b$, $\alpha$ and $\varepsilon$. Fig. 10 shows the original experimental data and the model prediction using the following parameter values:

$$n_{\min} = 600, \quad n_{\max} = 12000, \qquad b = 3\,\text{Å}, \quad \alpha = 0.46, \quad \varepsilon = 0.1\,k_B T. \tag{51}$$

Due to the large values of $n \in [n_{\min}, n_{\max}]$ and exponential decay in (43), it is sufficient to approximate the sum in (43) by considering only the term $n_0$ with maximum contribution. Good agreement is found between the model and experiments. In particular, the model

suggests four regimes: $0 \leq r \leq 1.56\,\mu$m at which the system demonstrates negligible stiffness, $1.56\,\mu\text{m} \leq r \leq 1.71\,\mu$m where the system can endure limited tensile force up to 65 pN with fixed $n = 600$, $1.71\,\mu\text{m} \leq r \leq 2.71\,\mu$m where the double helix unwinds and the force plateus, and $r \geq 2.71\,\mu$m where the force-bearing mechanism is reactivated at fixed $n = 12000$. It is of interest to note that the binding energy per unit length is given by $\varepsilon/\alpha b \approx 0.04\,\text{kcal}\,\text{mol}^{-1}\,\text{Å}^{-1}$. Taking the binding energy of a base pair to be $2k_BT$ (Liebl and Zacharias, 2017) and considering the base pair step length as 36 Å (Dong et al., 2018), the binding energy per unit length for the DNA is estimated to be $0.03\,\text{kcal}\,\text{mol}^{-1}\,\text{Å}^{-1}$. In Clausen-Schaumann et al. (2000), the data corresponding to single-stranded DNA were fitted using a modified freely-jointed chain model (Smith et al., 1996) with stretchable Kuhn segments of length 15 Å. Admittedly, the Kuhn length for the coil used in the present work is smaller, but considering the correct order of magnitude and the simplicity of our model, the parameters in (51) are deemed physically reasonable. The model is therefore able to capture the entire force-extension curve of the DNA which underwent conformation transition through unwinding of the double helix. It should be pointed out that in Fig. 10 the negative force in the experimental data near zero extension originates from the contact between the substrate and the AFM tip (Zhang and Zhang, 2003), not from the elasticity of the DNA chain. This part of the data is therefore not considered when comparison is made with the model. Also, while the stiffness of the AFM tip can play a significant role in the measurement (Florio and Puglisi, 2019; Bellino et al., 2019), its stiffness is likely large enough to allow the end-to-end distance to be prescribed (Eq. (42)) when empolying the grand canonical ensemble (Manca et al., 2013).

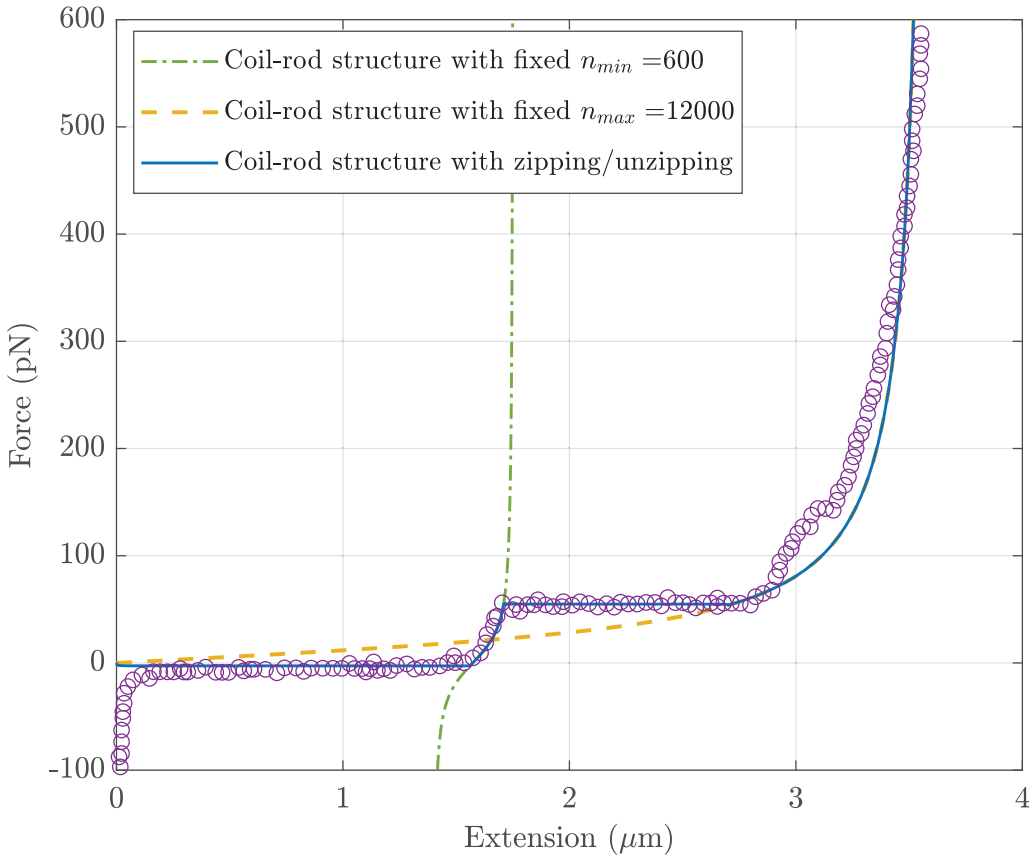


Figure 10: Force-extension curve of the double-stranded DNA in Clausen-Schaumann et al. (2000) (purple points). The solid curve is the prediction from the current model with the parameters in (51). The dashed lines represent results with fixed $n$ at $n_{\min} = 600$ and $n_{\max} = 12000$.

Some discussions are warranted on the modeling of unwinding/unfolding of biomacromolecules. It is acknowledged that there are other works that study the unwinding of double-stranded DNA via more elaborated description of intramolecular interactions. For example, in the model of denaturation by Theodorakopoulos et al. (2004), the interaction between a base pair is modelled via the Morse potential (Peyrard, 2004) and the DNA unzipping is

explained through the formation of domain walls in the one-dimensional lattice model. In comparison, in the present work the strength of interaction between the two DNA strands is represented by a single quantity, namely the binding energy $\varepsilon$. Despite the simplicity, it is encouraging to see that the model is capable of predicting the DNA unzipping phenomenon with physically reasonable parameter values. Although absent in Fig. 10, Fig. 8 shows the potential existence of sawtooth-like behaviour in the force-extension curve caused by unzipping. This type of phenomenon has been reported in the unfolding of proteins such as titin (Rief et al., 1997). A number of attempts have been made to model this phenomenon by considering folded and unfolded domains of a polymer structure. For example, Qi et al. (2006) investigated the effect of folded domains on the mechanics of biomacromolecules and their networks. The molecule is represented by a freely jointed chain or a worm-like chain while the Eyring model is used to capture the kinetics of unfolding. The model is able to achieve good fitting with the experimental data on the stretching of spectrin which exhibit sawtooth patterns. Based on the extensible freely jointed chain model (Manca et al., 2012), Manca et al. (2013) represented a polymer chain by connected domains each having a potential energy with two local minima. These two minima corresponds to two stable equilibrium states, one folded and the other unfolded. Monte-Carlo simulations using this model show sawtooth behaviour in the force-extension curves. Inspired by this work, Cannizzo et al. (2022) analyzed a discrete chain containing bistable units using three different models (Ising scheme, zipper model, and the stationary phase approximation) and studied the temperature effect on the force-extension response. De Tommasi et al. (2010) proposed a microstructure-based continuum model for the mechanics of spider silks, based on the original idea of De Tommasi et al. (2008). The material is assumed to consists of hard (folded) and soft (un-

folded) domains, which can transition between them. The total bearing force is taken to be the summation of the forces associated with the soft and hard domains. Via energy minimization of a two-state system, the same group (De Tommasi et al., 2013) also proposed a model for macromolecule unfolding and demonstrated its ability to match experimental data on the stretching of titin protein. These previous studies are valuable and provides different perspectives on how unwinding/unfolding may be modeled. Compared with these works, our approach to modeling unfolding is different in that: 1) we explicitly consider the rod element and its associated probability distribution; and 2) we employ the grand-canonical ensemble to statistically sample all the conformations corresponding to different number of segments in the coil. Since all the models are capable of reproducing experimental observations (with certain fitting parameters), it is of interest to conduct more examination in the future to compare their advantages and limitations.

## 7. Conclusion

Macroscopic responses of disordered biopolymer gels to external mechanical loading originate from the interaction between constituting macromolecules inside the network. To capture the presence of junction zones in disordered biopolymer gels, a coil-rod structure can be considered as a building block which consists of a freely jointed chain and a rigid rod segment. In this paper, the force-extension relations of the coil-rod structure are explored via a statistical mechanics formulation. The proposed formulation not only improves previous models in the literature but also unveils new features such as the requirement of compressive force to reach small end-to-end distance when the rod length is sufficiently large relative to the coil. When allowing the exchange between units in the rod and Kuhn segments in

the coil, the model is capable of capturing zipping/unzipping in the junction zone and the associated changes in the force-extension curve. The application of the current model is not merely limited to zipping/unzipping in the junction zones of biopolymer networks. It can also serve as a tool that provides a perspicuous explanation for the unwinding of interlocked strands, such as double helix structures. As an example of the application and based on availability of data, the coil-rod model is used to simulate the unwinding of double-stranded DNA subjected to external loading. The model is shown to be able to predict the transition of the double helical structure to single strands with satisfactory accuracy. An attempt is also made to implement the coil-rod model into the eight-chain model to predict the mechanical response of a coil-rod network under different loading conditions.

## Acknowledgements

TT acknowledges financial support from the Natural Sciences and Engineering Research Council of Canada (NSERC; Grant numbers: RGPIN-2018-04281, RGPAS-2018-522655) and Canada Research Chairs Program (Grant number: TIER1 2021-00023). HM acknowledges scholarship support from Alberta Innovates.

## References

Arruda, E.M., Boyce, M.C., 1993. A three-dimensional constitutive model for the large stretch behavior of rubber elastic materials. Journal of the Mechanics and Physics of Solids 41, 389 – 412. URL: http://www.sciencedirect.com/science/article/pii/0022509693900136, doi:https://doi.org/10.1016/0022-5096(93)90013-6.

Bellino, L., Florio, G., Puglisi, G., 2019. The influence of device handles in single-molecule experiments. Soft Matter 15, 8680–8690. doi:10.1039/c9sm01376h.

Buhot, A., Halperin, A., 2002. Extension behavior of helicogenic polypeptides. Macromolecules 35, 3238–3252. doi:10.1021/ma011631w.

Cannizzo, A., Bellino, L., Florio, G., Puglisi, G., Giordano, S., 2022. Thermal control of nucleation and propagation transition stresses in discrete lattices with non-local interactions and non-convex energy. European Physical Journal Plus 137. URL: https://doi.org/10.1140/epjp/s13360-022-02790-9, doi:10.1140/epjp/s13360-022-02790-9.

Carrillo, J.M.Y., MacKintosh, F.C., Dobrynin, A.V., 2013. Nonlinear elasticity: From single chain to networks and gels. Macromolecules 46, 3679–3692. doi:10.1021/ma400478f.

Clark, A., 1991. Structural and mechanical properties of biopolymer gels, in: Dickinson, E. (Ed.), Food Polymers, Gels and Colloids. Woodhead Publishing, pp. 322–338. URL: https://www.sciencedirect.com/science/article/pii/B978185573787750029X, doi:https://doi.org/10.1533/9781845698331.322.

Clark, A.H., Ross-Murphy, S.B., 1985. The concentration dependence of biopolymer gel modulus. British Polymer Journal 17, 164–168. URL: https://onlinelibrary.wiley.com/doi/abs/10.1002/pi.4980170214, doi:https://doi.org/10.1002/pi.4980170214, arXiv:https://onlinelibrary.wiley.com/doi/pdf/10.1002/pi.4980170214.

Clark, A.H., Ross-Murphy, S.B., 1987. Structural and mechanical properties of biopolymer gels, in: Biopolymers, Springer Berlin Heidelberg, Berlin, Heidelberg. pp. 57–192.

Clark, A.H., Ross-Murphy, S.B., 2009. Chapter 1 - biopolymer network assembly: Measurement and theory, in: Kasapis, S., Norton, I.T., Ubbink, J.B. (Eds.), Modern Biopolymer Science. Academic Press, San Diego, pp. 1–27. URL: https://www.sciencedirect.com/science/article/pii/B978012374195000001X, doi:https://doi.org/10.1016/B978-0-12-374195-0.00001-X.

Clausen-Schaumann, H., Rief, M., Tolksdorf, C., Gaub, H.E., 2000. Mechanical stability of single DNA molecules. Biophysical journal 78, 1997–2007.

De Tommasi, D., Millardi, N., Puglisi, G., Saccomandi, G., 2013. An energetic model for macromolecules unfolding in stretching experiments. Journal of the Royal Society Interface 10. doi:10.1098/rsif.2013.0651.

De Tommasi, D., Puglisi, G., Saccomandi, G., 2008. Localized versus diffuse damage in amorphous materials. Physical Review Letters 100, 1–4. doi:10.1103/PhysRevLett.100.085502.

De Tommasi, D., Puglisi, G., Saccomandi, G., 2010. Damage, self-healing, and hysteresis in spider silks. Biophysical Journal 98, 1941–1948. URL: http://dx.doi.org/10.1016/j.bpj.2010.01.021, doi:10.1016/j.bpj.2010.01.021.

De Tommasi, D., Puglisi, G., Saccomandi, G., 2015. Multiscale mechanics of macromolecular materials with unfolding domains. Journal of the Mechanics and Physics of Solids 78, 154–172. URL: https://www.sciencedirect.com/science/article/pii/S0022509615000332, doi:https://doi.org/10.1016/j.jmps.2015.02.002.

Dobrynin, A.V., Carrillo, J.M.Y., 2011. Universality in nonlinear elasticity of biological and polymeric networks and gels. Macromolecules 44, 140–146. doi:10.1021/ma102154u.

Doi, M., Kuzuu, N.Y., 1980. Nonlinear elasticity of rodlike macromolecules in condensed state. Journal of Polymer Science: Polymer Physics Edition 18, 409–419. URL: https://onlinelibrary.wiley.com/doi/abs/10.1002/pol.1980.180180301, doi:https://doi.org/10.1002/pol.1980.180180301, arXiv:https://onlinelibrary.wiley.com/doi/pdf/10.1002/pol.1980.180180301.

Dong, C., Zahir, N., Konstantopoulos, K., 2018. Biomechanics in Oncology. Advances in Experimental Medicine and Biology, Springer International Publishing. URL: https://books.google.co.uk/books?id=KDR1DwAAQBAJ.

Florio, G., Puglisi, G., 2019. Unveiling the influence of device stiffness in single macromolecule unfolding. Scientific Reports 9, 1–11. URL: http://dx.doi.org/10.1038/s41598-019-41330-x, doi:10.1038/s41598-019-41330-x.

Flory, P., 1969. Statistical Mechanics of Chain Molecules. Interscience Publishers. URL: https://books.google.com/books?id=EDZRAAAAMAAJ.

Giordano, S., 2018. Helmholtz and Gibbs ensembles, thermodynamic limit and bistability in polymer lattice models. Continuum Mechanics and Thermodynamics 30, 459–483. URL: https://doi.org/10.1007/s00161-017-0615-5, doi:10.1007/s00161-017-0615-5.

Higgs, P.G., Ball, R.C., 1989. Some ideas concerning the elasticity of biopolymer networks. Macromolecules 22, 2432–2437. URL: https://doi.org/10.1021/ma00195a073, doi:10.1021/ma00195a073, arXiv:https://doi.org/10.1021/ma00195a073.

Hill, T., 1986. An Introduction to Statistical Thermodynamics. Addison-Wesley series in chemistry, Dover Publications. URL: https://books.google.ca/books?id=pX4yxOHnWg8C.

Liebl, K., Zacharias, M., 2017. Unwinding induced melting of double-stranded dna studied by free energy simulations. The Journal of Physical Chemistry B 121, 11019–11030. URL: https://doi.org/10.1021/acs.jpcb.7b07701, doi:10.1021/acs.jpcb.7b07701, arXiv:https://doi.org/10.1021/acs.jpcb.7b07701. pMID: 29064703.

Magnenet, V., Schiavi-Tritz, J., Huselstein, C., Rahouadj, R., 2012. Constitutive equations for Ca2+ -alginate gels. Journal of the Mechanical Behavior of Biomedical Materials 5, 90–98. URL: https://www.sciencedirect.com/science/article/pii/S175161611100213X, doi:https://doi.org/10.1016/j.jmbbm.2011.08.009.

Manca, F., Giordano, S., Palla, P.L., Cleri, F., Colombo, L., 2013. Two-state theory of single-molecule stretching experiments. Physical Review E - Statistical, Nonlinear, and Soft Matter Physics 87, 1–6. doi:10.1103/PhysRevE.87.032705.

Manca, F., Giordano, S., Palla, P.L., Zucca, R., Cleri, F., Colombo, L., 2012. Elasticity of flexible and semiflexible polymers with extensible bonds in the Gibbs and Helmholtz ensembles. Journal of Chemical Physics 136, 154906. doi:10.1063/1.4801656.

Marko, J.F., Siggia, E.D., 1995. Stretching dna. Macromolecules 28, 8759–8770. URL: https://doi.org/10.1021/ma00130a008, doi:10.1021/ma00130a008, arXiv:https://doi.org/10.1021/ma00130a008.

McEvoy, H., Ross-Murphy, S., Clark, A., 1985. Large deformation and ultimate

properties of biopolymer gels: 1. single biopolymer component systems. Polymer 26, 1483–1492. URL: https://www.sciencedirect.com/science/article/pii/0032386185900813, doi:https://doi.org/10.1016/0032-3861(85)90081-3.

Moe, S.T., Draget, K.I., Skjåk-Bræk, G., Simdsrød, O., 1992. Temperature dependence of the elastic modulus of alginate gels. Carbohydrate Polymers 19, 279–284. URL: https://www.sciencedirect.com/science/article/pii/014486179290081Z, doi:https://doi.org/10.1016/0144-8617(92)90081-Z.

Moresi, M., Bruno, M., 2007. Characterisation of alginate gels using quasi-static and dynamic methods. Journal of Food Engineering 82, 298–309. URL: https://www.sciencedirect.com/science/article/pii/S0260877407001227, doi:https://doi.org/10.1016/j.jfoodeng.2007.02.040.

Nishinari, K., 2007. Rheological and related studies on industrially important polysaccharides and proteins. Journal of Central South University of Technology 14, 498–504.

Nishinari, K., Koide, S., Ogino, K., 1985. On the temperature dependence of elasticity of thermo-reversible gels. Journal de Physique 46, 793–797. URL: https://hal.archives-ouvertes.fr/jpa-00210021, doi:10.1051/jphys:01985004605079300.

Peyrard, M., 2004. Nonlinear dynamics and statistical physics of DNA. Nonlinearity 17. doi:10.1088/0951-7715/17/2/R01.

Qi, H.J., Ortiz, C., Boyce, M.C., 2006. Mechanics of biomacromolecular networks containing folded domains. Journal of Engineering Materials and Technology 128, 509–518. doi:10.1115/1.2345442.

Rief, M., Gautel, M., Oesterhelt, F., Fernandez, J.M., Gaub, H.E., 1997. Reversible unfolding of individual titin immunoglobulin domains by AFM. Science 276, 1109–1112. doi:10.1126/science.276.5315.1109.

Smith, S.B., Cui, Y., Bustamante, C., 1996. Overstretching B-DNA: the elastic response of individual double-stranded and single-stranded DNA molecules. Science 271, 795–799.

Theodorakopoulos, N., Peyrard, M., MacKay, R.S., 2004. Nonlinear structures and thermodynamic instabilities in a one-dimensional lattice system. Physical Review Letters 93, 1–4. doi:10.1103/PhysRevLett.93.258101.

Titantah, J.T., Pierleoni, C., Ryckaert, J.P., 1999. Different statistical mechanical ensembles for a stretched polymer. Phys. Rev. E 60, 7010–7021. URL: https://link.aps.org/doi/10.1103/PhysRevE.60.7010, doi:10.1103/PhysRevE.60.7010.

Treloar, L., 1975. The Physics of Rubber Elasticity. Oxford Classic Texts in the Physical Sciences, Oxford University Press, USA. URL: https://books.google.com/books?id=EfCZXXKQ50wC.

Treloar, L.R.G., 1946. The statistical length of long-chain molecules. Trans. Faraday Soc. 42, 77–82. URL: http://dx.doi.org/10.1039/TF9464200077, doi:10.1039/TF9464200077.

Wang, H., Xu, X., 2020. Continuum elastic models for force transmission in biopolymer gels. Soft Matter 16, 10781–10808. URL: http://dx.doi.org/10.1039/D0SM01451F, doi:10.1039/D0SM01451F.

Wang, W., Zhang, Y., Liu, W., 2017. Bioinspired fabrication of high strength hydrogels from non-covalent interactions. Progress in Polymer Science 71, 1–25. URL: http://dx.

doi.org/10.1016/j.progpolymsci.2017.04.001, doi:10.1016/j.progpolymsci.2017.04.001.

Weiner, J.H., 1982. Use of s = k log p for stretched polymers. Macromolecules 15, 542–544. URL: https://doi.org/10.1021/ma00230a064, doi:10.1021/ma00230a064, arXiv:https://doi.org/10.1021/ma00230a064.

Winkler, R.G., 2010. Equivalence of statistical ensembles in stretching single flexible polymers. Soft Matter 6, 6183–6191. URL: http://dx.doi.org/10.1039/C0SM00488J, doi:10.1039/C0SM00488J.

Xu, X., Safran, S.A., 2015. Nonlinearities of biopolymer gels increase the range of force transmission. Phys. Rev. E 92, 032728. URL: https://link.aps.org/doi/10.1103/PhysRevE.92.032728, doi:10.1103/PhysRevE.92.032728.

Yamakawa, H., 1971. Modern theory of polymer solutions. Harper & Row.

Zhang, J., Daubert, C.R., Allen Foegeding, E., 2007. A proposed strain-hardening mechanism for alginate gels. Journal of Food Engineering 80, 157–165. URL: https://www.sciencedirect.com/science/article/pii/S026087740600402X, doi:https://doi.org/10.1016/j.jfoodeng.2006.04.057.

Zhang, W., Zhang, X., 2003. Single molecule mechanochemistry of macromolecules. Progress in Polymer Science (Oxford) 28, 1271–1295. doi:10.1016/S0079-6700(03)00046-7.